

Covert Communication in Hybrid Microwave/mmWave A2G Systems with Transmission Mode Selection

Wenhao Zhang, *Student Member, IEEE*, Ji He, *Member, IEEE*, Yulong Shen, *Member, IEEE*, Xiaohong Jiang, *Senior Member, IEEE*,

Abstract—This paper investigates the covert communication in an air-to-ground (A2G) system, where a UAV (Alice) can adopt the omnidirectional microwave (OM) or directional mmWave (DM) transmission mode to transmit covert data to a ground user (Bob) while suffering from the detection of an adversary (Willie). For both the OM and DM modes, we first conduct theoretical analysis to reveal the inherent relationship between the transmit rate/transmit power and basic covert performance metrics in terms of detection error probability (DEP), effective covert rate (ECR), and covert Shannon capacity (CSC). To facilitate the transmission mode selection at Alice, we then explore the optimization of transmit rate and transmit power for ECR/CSC maximization under the OM and DM modes, and further propose a hybrid OM/DM transmission mode which allows the UAV to adaptively select between the OM and DM modes to achieve the maximum ECR and CSC at a given location of UAV. Finally, extensive numerical results are provided to illustrate the covert performances of the concerned A2G system under different transmission modes, and demonstrate that the hybrid OM/DM transmission mode outperforms the pure OM or DM mode in terms of covert performance.

Index Terms—air to ground communication, UAV, covert communication, microwave, mmWave.

I. INTRODUCTION

With the ever-increasing applications of wireless networks, an unprecedented amount of private and sensitive information is transferred over the wireless medium. However, the broadcast characteristic of wireless channels will lead to serious security risks. Although cryptography is the well-known security method, it has been demonstrated that even the most robust cryptography is at risk of being brutally cracked by quantum computing [1]. As an alternative approach, physical layer security can achieve information-theoretic security by exploiting the inherent physical layer randomness of wireless channels [2]. Recently, covert communication has been regarded as a new security paradigm to hide the communication process itself to achieve a stronger level of security [3].

Bash et al. first derived the information theory limitation called square root law (SRL) for covert communication [4], pointing out that under the additive white Gaussian noise (AWGN) channel, Alice can only reliably and covertly send

$\mathcal{O}(\sqrt{n})$ bits to Bob over n channel uses. Subsequently, the fundamental limit of covert communication has been further studied under various wireless channels, including binary symmetric channels [5], discrete memory-less channels [6], and multiple input multiple output (MIMO) AWGN channels [7]. Following this line, extensive research works have been dedicated to the study of covert communication in various network scenarios. According to the movability of network nodes, these available works can be classified as studies for network scenarios with fixed nodes and studies for network scenarios with mobile nodes.

For the network scenarios with fixed nodes, the authors in [8] first proved that a nonzero covert rate is possible over the AWGN channels and Rayleigh channels regardless of the finite or infinite channel use. Based on the results, the optimal power adaptation schemes were designed in [9]. Considering the channel uncertainty, the work [10] reveals the fundamental difference in the design of covert transmission schemes between the case of quasi-static fading channel and the case of non-fading AWGN channel [11]. The jamming-assisted covert communication was also explored in different network scenarios, including the ones with full-duplex jamming receiver [12], the ones with Poisson point distributed jammer [13], the ones with randomly located warden [14], the ones with two-hop relaying [15], and the ones with intelligent reflecting surface (IRS) technology [16], [17]. Notice that the millimeter-wave (mmWave) technology can bring high bandwidth, the covert communications with mmWave has been examined in some recent works. The authors in [18] first considered a mmWave communication system with dual independent antenna arrays, and proposed a covert transmission scheme where one antenna array is used to form a beam towards Bob for data transmission and the other is used for jamming. The covert rate maximization in mmWave system was investigated in [19] through the joint optimization of beam training duration, training power and transmission power. A multi-user beam training strategy was proposed in [20] to maximize the effective covert throughput. Besides, the authors in [21] considered a full-duplex covert mmWave communications scenario, and explored the maximization of achievable covert rate by jointly optimizing the beamforming, transmit power, and jamming power.

For the mobile node network scenario, the impact of node mobility on the covert performance in the mobile Ad Hoc network was first studied in [22]. Considering the UAV-

W. Zhang and X. Jiang are with the School of System Information Science, Future University Hakodate, Hakodate, 041-8655 Japan (e-mail: h1zhangwenhao@gmail.com; jiang@fun.ac.jp).

J. He and Y. Shen are with the School of Computer Science and Technology, Xidian University, Xi'an, 710071 China (e-mail: gary-hej1991@gmail.com; ylshen@mail.xidian.edu.cn).

TABLE I
LIST OF NOTATIONS

Notation	Description
P_a, d_{ij}, h_i	Transmission power of Alice, Distance between nodes i and j , height of node i
$d_{aw}^{\min}, d_{aw}^{\max}$	Minimum distance and maximum distance between Alice and Willie
$\mathbb{A} \in \{M, S\}$	Main lobe and side lobe, respectively
$\mathbb{B} \in \{L, N\}$	LoS channel and NLoS channel, respectively
$\mathbb{C} \in \{o, d\}$	OM transmission mode and DM transmission mode, respectively
G_{ij}, G_i^M, G_i^S	Total antenna gains of link $i \rightarrow j$, main lobe gain, side lobe gain
P_{ij}^L, P_{ij}^N	Probability that the channel mode of link $i \rightarrow j$ is LoS link and NLoS link, respectively
$H_{ij}^{\mathbb{C}, \mathbb{B}}, h_{ij}^{\mathbb{C}, \mathbb{B}}, L_{ij}^{\mathbb{C}, \mathbb{B}}$	Channel coefficient, small scaling fading coefficient and path loss of link $i \rightarrow j$, respectively
$\alpha_{\mathbb{B}}, \beta_{\mathbb{B}}, S_{\mathbb{B}}, k_{\mathbb{B}}$	Path-loss exponent, path-loss coefficient, Nakagami fading parameter, Rician factor of \mathbb{B} , respectively
$\theta_i, \theta_i^h, \theta_i^{e/d}, \varphi_i$	Elevation angle of UAV relative to node i , half-power beamwidth for the azimuth orientation in the horizontal direction of node i , half-power beamwidth for the elevation/depression angles of node i , azimuth orientation in the vertical direction of node i relative to UAV, respectively
$\sigma_b^2, \sigma_w^2, \hat{\sigma}_n^2$	Noise power of Bob, noise power of Willie, nominal noise power of Willie
$\epsilon, \gamma_{th}, R_b$	Coverttness constraint, outage probability threshold, target rate, respectively.

with a horizontal trajectory around the surveillance area at a fixed height h_a . We let d_{ij} denote the distance between node i and node j for $i, j \in \{a, b, w\}$. To prevent the UAV from being detected by vision or radar, there exists a minimum distance constraint d_{aw}^{\min} between Alice and Willie. Besides, due to the finite resolution of the UAV's imaging equipment, a maximum distance constraint d_{aw}^{\max} is essential.

B. Antenna Gains

Because UAV moves in 3D space, we adopt the 3D sectorized antenna pattern as [39], [40], which is essential to model the links from air to ground. As shown in Fig. 1, θ_i^h is the half-power beamwidth for the azimuth orientation in the horizontal direction, θ_i^e (resp. θ_i^d) is the half-power beamwidth for the elevation (resp. depression) angles in the ground or air node i . Considering the antenna gain G_i^M within the half-power beamwidth (i.e., main lobe) and gain G_i^S outside the half-power beamwidth (i.e., side lobe), the total directivity gain of DM for link $i \rightarrow j$ is determined as $G_{ij} = G_i^{\mathbb{A}} G_j^{\mathbb{A}}$, where $\mathbb{A} \in \{M, S\}$. To improve the signal quality at Bob, Alice dynamically adjusts the steering orientation of the antenna array toward Bob, such that she can maximize antenna array gain G_a^M . Thus, the directional antenna gain of Alice \rightarrow Bob link is determined as $G_{ab} = G_a^M G_b^{\mathbb{A}}$. Note that in the process of Alice's movement, Willie may be located in the half-power beamwidth direction of the antenna array of Alice \rightarrow Bob link (i.e., $\pi - \varphi_w - \varphi_b \leq \theta_a^d$) and the antenna array gain of Alice for Willie is the main lobe gain G_a^M , otherwise, the side lobe

gain G_a^S . Thus, the antenna gain of Alice \rightarrow Willie link is determined as

$$G_{aw} = G_w^{\mathbb{A}} \times \begin{cases} G_a^M, & \pi - \varphi_w - \varphi_b \leq \theta_a^d, \\ G_a^S, & \text{otherwise.} \end{cases} \quad (1)$$

Considering an actual situation, we adopt a uniform planar square array (UPA) to model the sectorized pattern at node j (here, $j \in \{b, w\}$). The directional antenna gain and the associated probability can be approximated as

$$G_j^{\mathbb{A}} = \begin{cases} G_j^M = \mathcal{N}_j, & P_j^M = \frac{\theta_j^h}{2\pi} \times \frac{\theta_j^e}{\pi}, \\ G_j^S = \frac{\sqrt{\mathcal{N}_j - \frac{\sqrt{3}}{2\pi}} \mathcal{N}_j \sin\left(\frac{3\pi}{2\sqrt{\mathcal{N}_j}}\right)}{\sqrt{\mathcal{N}_j - \frac{\sqrt{3}}{2\pi}} \sin\left(\frac{3\pi}{2\sqrt{\mathcal{N}_j}}\right)}, & P_j^S = 1 - \frac{\theta_j^h}{2\pi} \times \frac{\theta_j^e}{\pi}, \end{cases} \quad (2)$$

where \mathcal{N}_j denotes the number of antenna elements at the node j , $P_j^{\mathbb{A}}$ denotes the associated probability.

C. Propagation Model

To characterize the A2G wireless channel feature, the channel from UAV to Bob (Willie) is modeled as the combination of NLoS and LoS channels. Specifically, we let $P_{aj}^{\mathbb{B}}$ ($\mathbb{B} \in \{L, N\}, j \in \{b, w\}$) denotes the probability the channel from the UAV to node j is the LoS or NLoS, where $P_{aj}^L = (1 + \sigma \exp(-f[\theta_j - \sigma]))^{-1}$ and $P_{aj}^N \triangleq 1 - P_{aj}^L$ as [41], [42], where $\theta_j = \frac{180}{\pi} \arcsin\left(\frac{h_a}{d_{aj}}\right)$ is the degree of the elevation angle for node j relative to UAV, $d_{aj} = \sqrt{(x_a - x_j)^2 + h_a^2}$ is the distance between UAV and node j , σ and f are the S-curve parameters that depend on the communication environment. In this work, we consider both the large scale fading and small scale fading. Thus, the channel coefficient for link $a \rightarrow j$ is denoted as $H_{aj}^{\mathbb{C}, \mathbb{B}} = h_{aj}^{\mathbb{C}, \mathbb{B}} \sqrt{L_{aj}^{\mathbb{C}, \mathbb{B}}}$, where $\mathbb{C} \in \{o, m\}$ denotes adopting the OM or DM, $h_{aj}^{\mathbb{C}, \mathbb{B}}$ and $L_{aj}^{\mathbb{C}, \mathbb{B}}$ denote the channel fading coefficient and path loss, respectively. We have $L_{aj}^{\mathbb{C}, \mathbb{B}} = \beta_{\mathbb{B}}^{\mathbb{C}} d_{aj}^{-\alpha_{\mathbb{B}}^{\mathbb{C}}}$, where $\beta_{\mathbb{B}}^{\mathbb{C}}$ and $\alpha_{\mathbb{B}}^{\mathbb{C}}$ are the constant coefficient and path-loss exponent, respectively.

1) *Small scaling fading of Microwave channel*: Due to the possible combination of LoS and multipath scatterers of NLoS, the microwave channels are modeled as Rician fading to characterize the propagation effect. Thus, the fading coefficient $h_{ij}^{o, \mathbb{B}}$ can be described as

$$h_{ij}^{o, \mathbb{B}} = \sqrt{\frac{k_{\mathbb{B}}}{k_{\mathbb{B}} + 1}} \hat{h}_{ij} + \sqrt{\frac{1}{k_{\mathbb{B}} + 1}} \tilde{h}_{ij}, \quad (3)$$

where $|\hat{h}_{ij}| = 1$ and $\tilde{h}_{ij} \sim \mathcal{CN}(0, 1)$ denote the components of LoS channel and NLoS Rayleigh fading, respectively, $k_{\mathbb{B}}$ denotes the Rician factor which is determined as [43], [44]

$$k_{\mathbb{B}}(\theta_j) = \begin{cases} \eta_1 \exp(\eta_2 \theta_j), & \text{LoS,} \\ 0, & \text{NLoS,} \end{cases} \quad (4)$$

η_1 and η_2 are constant coefficients with $\eta_1 = k_0$ and $\eta_2 = \frac{2}{\pi} \ln\left(\frac{k_{\frac{\pi}{2}}}{k_0}\right)$, $k_0 = k_{\mathbb{B}}(0)$ and $k_{\frac{\pi}{2}} = k_{\mathbb{B}}(\frac{\pi}{2})$ are depending on the specific environment. Thus, the fading coefficient $|h_{ij}^{o, \mathbb{B}}|^2$ follows a non-central chi-squared distribution with two degrees

of freedom and $\mathbb{E}[|h_{ij}^{o,\mathbb{B}}|^2] = 1$, the probability density function (PDF) of $|h_{ij}^{o,\mathbb{B}}|^2$ is expressed as [45]

$$f_{|h_{ab}^{o,\mathbb{B}}|^2}(x) = (k_{\mathbb{B}} + 1)e^{-k_{\mathbb{B}} - (k_{\mathbb{B}} + 1)x} I_0(2\sqrt{k_{\mathbb{B}}(k_{\mathbb{B}} + 1)x}), \quad (5)$$

where $I_0(\cdot)$ is the modified Bessel function of the first kind and zeroth order, and the corresponding CDF of $|h_{ij}^{o,\mathbb{B}}|^2$ can be expressed as [44], [45]

$$F_{|h_{ij}^{o,\mathbb{B}}|^2}(x) = 1 - Q_1(\sqrt{2k_{\mathbb{B}}}, \sqrt{2(k_{\mathbb{B}} + 1)x}), \quad (6)$$

where $Q_1(a, b)$ is the standard Marcum-Q function which is

$$Q_1(a, b) = \int_b^\infty x I_0(ax) \exp\left(-\frac{x^2 + a^2}{2}\right) dx. \quad (7)$$

$I_0(\cdot)$ is mentioned above.

2) *Small scaling fading of mmWave channel*: mmWave channels are characterized by the Nakagami-m fading with shape parameter $S_{\mathbb{B}} \geq 1/2$ and scale parameter $\Omega = \mathbb{E}[|h_{ij}^{d,\mathbb{B}}|^2] = 1$ as [40], [41], [46]. Thus, the fading coefficient $|h_{ij}^{d,\mathbb{B}}|^2$ follows a normalized gamma distribution with shape and scale parameters of $S_{\mathbb{B}}$ and $1/S_{\mathbb{B}}$. Therefore, the PDF is given by [18], [45]

$$f_{|h_{ab}^{d,\mathbb{B}}|^2}(x) = S_{\mathbb{B}}^x x^{S_{\mathbb{B}}-1} e^{-S_{\mathbb{B}}x} / \Gamma(S_{\mathbb{B}}). \quad (8)$$

According to [46, Lemma 6] and Alzer's lemma [47], the CDF of a normalized gamma RV is tightly approximated by $[1 - \exp(-\xi_{\mathbb{B}}x)]^{S_{\mathbb{B}}}$ where $\xi_{\mathbb{B}} = S_{\mathbb{B}}(S_{\mathbb{B}}!)^{-1/S_{\mathbb{B}}}$. By applying the binomial theorem assuming $S_{\mathbb{B}}$ is an integer [46], the CDF of $|h_{ij}^{d,\mathbb{B}}|^2$ is given by

$$F_{|h_{ij}^{d,\mathbb{B}}|^2}(x) = \sum_{r=0}^{S_{\mathbb{B}}} \binom{S_{\mathbb{B}}}{r} (-1)^r e^{-r\xi_{\mathbb{B}}x}. \quad (9)$$

D. Noise Uncertainty Model

In practice, the background noise is uncertain due to its complex composition (including thermal noise, quantization noise, imperfect filters, ambient wireless signals, etc.), dynamic environment and calibration error. Therefore, it is practical to use noise uncertainty to realize covert communication in mobile communication scenarios. In this work, we adopt the typical bounded noise uncertainty model [48], where the exact noise power of node i σ_i^2 lies in a finite range around the nominal noise power $\hat{\sigma}_n^2$, then, the log-uniform distribution of σ_i^2 for the bounded uncertainty model is given by

$$f_{\sigma_i^2}(x) = \begin{cases} \frac{1}{2 \ln(\rho)x}, & \frac{1}{\rho} \hat{\sigma}_n^2 \leq \sigma_i^2 \leq \rho \hat{\sigma}_n^2, \\ 0, & \text{otherwise,} \end{cases} \quad (10)$$

where ρ is the parameter that quantifies the level of the uncertainty.

E. Definitions

Some basic definitions involved in this work are as follows.

Detection Error Probability (DEP) P_{ew} : Let H_0 (the null hypothesis and H_1 (the alternative hypothesis) denote that Alice does not transmit and transmits covert information, respectively, let D_0 and D_1 respectively indicate the judgment

of Willie that UAV is transmitting or not transmitting covert information. The DEP P_{ew} is defined as the probability that Willie makes a wrong decision on whether or not UAV is transmitting covert messages, which is expressed as

$$P_{ew} = P_{FA} + P_{MD}, \quad (11)$$

where $P_{FA} = \mathbb{P}(D_1|H_0)$ is the false alarm probability that Willie is in favor of H_1 while H_0 is true, $P_{MD} = \mathbb{P}(D_0|H_1)$ is the missed detection probability that Willie is in favor of H_0 while H_1 is true.

Outage Probability P_{out} : The outage probability P_{out} is defined as the probability that the channel capacity $C_{ab} = W \log_2(1 + \gamma_{ab})$ cannot support a given target transmission rate R_b , i.e., $P_{out} = \mathbb{P}(C_{ab} < R_b)$ which can also be denoted as $P_{out} = \mathbb{P}(\gamma_{ab} < \gamma_{th})$ where W is the bandwidth of $a \rightarrow b$ link, γ_{ab} is the SNR, and γ_{th} is the threshold of SNR which can be calculated as $\gamma_{th} = 2^{\frac{R_b}{W}} - 1$.

Effective Covert Rate (ECR) R_{ab} : The effective covert rate R_{ab} is defined the average *successfully* transmitted amount of information, which can be denoted as $R_{ab} = R_b \times (1 - P_{out})$, where R_b is the target covert transmission rate and P_{out} is the outage probability.

Covert Shannon (Ergodic) Capacity (CSC) C_{ab} : The covert Shannon capacity is defined as the maximum value of the time average rate of messages delivered from transmitter to the destination, which is expressed as $C_{ab} = \mathbb{E}[W \log_2(1 + \gamma_{ab})]$, where W is the bandwidth and γ_{ab} is the SNR.

III. TRANSMISSION MODE AND DETECTION STRATEGY

In this section, we first introduce two transmission modes of UAV (OM transmission mode and DM transmission mode), and then present the detection strategy at Willie.

A. OM Transmission Mode

When UAV adopts the OM transmission mode, the signals $y_b(k)$ ($k \in \{1, 2, \dots, N\}$) received by Bob at k -th channel use is given by

$$y_b^o(k) = \sqrt{P_a} H_{ab}^{o,\mathbb{B}} x_c(k) + n_b(k), \quad (12)$$

and the signals $y_w^o(k)$ received by Willie is given by

$$y_w^o(k) = \sqrt{P_a} H_{aw}^{o,\mathbb{B}} x_c(k) + n_w(k). \quad (13)$$

where x_c is the desired signal, which following a zero-mean Gaussian distribution, i.e., $\mathbb{E}[x_c(k)^2] = 1$. Besides, $n_b(k)$ and $n_w(k)$ are the received noise power at Bob and Willie, respectively, and the PDF is given by (10).

B. DM Transmission Mode

When UAV adopts the DM transmission mode, the signals $y_b^d(k)$ received by Bob at the k -th ($k \in \{1, 2, \dots, N\}$) channel use is given by

$$y_b^d(k) = \sqrt{P_a G_{ab}} H_{ab}^{d,\mathbb{B}} x_c(k) + n_b(k), \quad (14)$$

and the signals $y_w^d(k)$ received by Willie is given by

$$y_w^d(k) = \sqrt{P_a G_{aw}} H_{aw}^{d,\mathbb{B}} x_c(k) + n_w(k), \quad (15)$$

The desired signal x_c and noise power obey the same distribution as the OM transmission mode.

C. Detection Strategy at Willie

Based on the observations over all time slots, Willie attempts to determine whether Alice conducts transmission or not. According to [11], the optimal decision rule at Willie to minimize the detection error probability is determined as

$$T_w = \lim_{N \rightarrow \infty} \frac{P_{tol}}{N} \underset{H_0}{\geq} \tau, \quad (16)$$

where $P_{tol} = \sum_{k=1}^N |y_w(k)|^2$ is the total power received by Willie in a given block, τ is the decision threshold, and N is the total number of channel uses in a block. According to (13), when Alice adopts the OM transmission mode, the received signal $y_w^o(k)$ at Willie is given by

$$T_w^o = \begin{cases} \sigma_w^2, & H_0 \\ P_a L_{aw}^{o,\mathbb{B}} |h_{aw}^{o,\mathbb{B}}|^2 + \sigma_w^2, & H_1 \end{cases} \quad (17)$$

Similarly, according to (15), when Alice adopts the DM transmission mode, the received signal $y_w^d(n)$ received at Willie is given by

$$T_w^d = \begin{cases} \sigma_w^2, & H_0 \\ P_a G_{aw} L_{aw}^{d,\mathbb{B}} |h_{aw}^{d,\mathbb{B}}|^2 + \sigma_w^2, & H_1 \end{cases} \quad (18)$$

IV. COVERT PERFORMANCE ANALYSIS UNDER THE OM TRANSMISSION MODE

In this section, we derive the optimal detection threshold and the corresponding minimum DEP at Willie, as well as the expected minimum DEP from Alice's perspective, lastly, the ECR and CSC under the OM transmission mode.

A. Detection Error Probability

To determine the DEP at Willie, we first analyze the false alarm probability and the missed detection probability. Based on (16) and (17), the false alarm probability P_{FA}^o is given by

$$P_{FA}^o = \mathbb{P}(T_w^o > \tau | H_0) = \mathbb{P}\left(\sigma_w^2 \frac{\chi_{2N}^2}{N} > \tau\right), \quad (19)$$

where χ_{2N}^2 denotes a random value that follows chi-squared distribution with $2N$ degrees of freedom. From the strong law of large numbers, we know that χ_{2N}^2/N converges to 1. Based on Lebesgue's Dominated Convergence Theorem [49], P_{FA}^o can be derived as

$$P_{FA}^o = \mathbb{P}(\sigma_w^2 > \tau) = \begin{cases} 1, & \tau < \frac{\sigma_w^2}{\rho}, \\ 1 - \frac{\ln(\rho\tau) - \ln(\hat{\sigma}_n^2)}{2 \ln(\rho)}, & \frac{\sigma_w^2}{\rho} \leq \tau \leq \rho \hat{\sigma}_n^2, \\ 0, & \tau > \rho \hat{\sigma}_n^2. \end{cases} \quad (20)$$

Similarly, the missed detection probability can be derived as

$$P_{MD}^o = \mathbb{P}(T_w^o > \tau | H_1) = \mathbb{P}(k_a^o + \sigma_w^2 < \tau) = \begin{cases} 1, & \tau > k_a^o + \rho \hat{\sigma}_n^2, \\ \frac{\ln(\rho(\tau - k_a^o)) - \ln(\hat{\sigma}_n^2)}{2 \ln(\rho)}, & k_a^o + \frac{\sigma_w^2}{\rho} \leq \tau \leq k_a^o + \rho \hat{\sigma}_n^2, \\ 0, & \tau < k_a^o + \frac{\sigma_w^2}{\rho}, \end{cases} \quad (21)$$

where $k_a^o = P_a L_{aw}^{o,\mathbb{B}} |h_{aw}^{o,\mathbb{B}}|^2$. According to (20) and (21), we can analyze the optimal detection threshold and the minimization DEP for Willie under OM transmission mode as follows.

Lemma 1. When Alice adopts the OM transmission mode, the optimal threshold τ^* for Willie's detector is in the interval

$$\tau^* \in \begin{cases} [\rho \hat{\sigma}_n^2, k_a^o + \frac{\sigma_w^2}{\rho}], & \rho \hat{\sigma}_n^2 < k_a^o + \frac{\sigma_w^2}{\rho}, \\ k_a^o + \frac{\sigma_w^2}{\rho}, & \rho \hat{\sigma}_n^2 \geq k_a^o + \frac{\sigma_w^2}{\rho}, \end{cases} \quad (22)$$

and the corresponding minimum DEP $P_{ew}^{*,o}$ is given as

$$P_{ew}^{*,o} = \begin{cases} 0, & \rho \hat{\sigma}_n^2 < k_a^o + \frac{\sigma_w^2}{\rho}, \\ 1 - \frac{\ln(\rho k_a^o + \hat{\sigma}_n^2) - \ln(\hat{\sigma}_n^2)}{2 \ln(\rho)}, & \rho \hat{\sigma}_n^2 \geq k_a^o + \frac{\sigma_w^2}{\rho}, \end{cases} \quad (23)$$

where $k_a^o = P_a L_{aw}^{o,\mathbb{B}} |h_{aw}^{o,\mathbb{B}}|^2$, ρ and $\hat{\sigma}_n^2$ are the parameter that quantifies the size of the uncertainty and nominal noise power, respectively, defined in II-D.

Proof. To find the optimal threshold, we consider the optimization problem $\min_{\tau} P_{ew}^o = P_{FA}^o + P_{MD}^o$. According to (20) and (21), the following two cases are considered.

Case I: When $\rho \hat{\sigma}_n^2 < k_a^o + \frac{\sigma_w^2}{\rho}$, for any $\tau \in [\rho \hat{\sigma}_n^2, k_a^o + \frac{\sigma_w^2}{\rho}]$, we have $P_{ew}^o = P_{FA}^o + P_{MD}^o = 0$.

Case II: When $\rho \hat{\sigma}_n^2 \geq k_a^o + \frac{\sigma_w^2}{\rho}$, the DEP $P_{ew}^o = P_{FA}^o + P_{MD}^o$ can be written as

$$P_{ew}^o = \begin{cases} 1, & \tau < \frac{\sigma_w^2}{\rho}, & (24a) \\ 1 - \frac{\ln(\rho\tau) - \ln(\hat{\sigma}_n^2)}{2 \ln(\rho)}, & \frac{\sigma_w^2}{\rho} \leq \tau < k_a^o + \frac{\sigma_w^2}{\rho}, & (24b) \\ 1 - \frac{\ln(\tau) - \ln(\tau - k_a^o)}{2 \ln(\rho)}, & k_a^o + \frac{\sigma_w^2}{\rho} \leq \tau \leq \rho \hat{\sigma}_n^2, & (24c) \\ \frac{\ln(\rho(\tau - k_a^o)) - \ln(\hat{\sigma}_n^2)}{2 \ln(\rho)}, & \rho \hat{\sigma}_n^2 < \tau \leq k_a^o + \rho \hat{\sigma}_n^2, & (24d) \\ 1, & \tau > k_a^o + \rho \hat{\sigma}_n^2. & (24e) \end{cases}$$

then we can see from (24b), when $\frac{\sigma_w^2}{\rho} \leq \tau < k_a^o + \frac{\sigma_w^2}{\rho}$, P_{ew}^o is a decreasing function of τ . Thus, when $\tau = k_a^o + \frac{\sigma_w^2}{\rho}$, P_{ew}^o gets the minimum value which equals to (24c). From (24d), when $\rho \hat{\sigma}_n^2 < \tau \leq k_a^o + \rho \hat{\sigma}_n^2$, P_{ew}^o is an increasing function of τ . Thus, when $\tau = \rho \hat{\sigma}_n^2$, P_{ew}^o gets the minimum value which equals to (24c). Overall, the DEP gets the minimum value $P_{ew}^{*,o}$ for Willie if and only if $\tau \in [k_a^o + \frac{\sigma_w^2}{\rho}, \rho \hat{\sigma}_n^2]$. After deriving the first-order derivative of P_{ew}^o with respect to τ , we have

$$\frac{\partial P_{ew}^o}{\partial \tau} = \frac{k_a^o}{2\tau(\tau - k_a^o) \ln(\rho)} > 0. \quad (25)$$

Obviously, P_{ew}^o is monotonically increasing in the interval. Thus, the optimal threshold τ^* for Willie is $\tau = k_a^o + \frac{\sigma_w^2}{\rho}$ and the corresponding minimum DEP $P_{ew}^{*,o}$ is

$$P_{ew}^{*,o} = 1 - \frac{\ln(\rho k_a^o + \hat{\sigma}_n^2) - \ln(\hat{\sigma}_n^2)}{2 \ln(\rho)}. \quad (26)$$

Based on Case I and Case II, we have (22) and (23). ■

Since only the statistical channel static information of Alice \rightarrow Willie, we use the expected measure of $P_{ew}^{*,o}$ to evaluate the covertness. From (23), we note that $\mathbb{E}[P_{ew}^{*,o}]$ is related to the numerical integration of $|h_{aw}^{o,\mathbb{B}}|^2$. To this end, we first present the following lemma.

$$\mathbb{E}[P_{ew}^{*,o}] = \sum_{\mathbb{B} \in \{L, N\}} P_{aw}^{\mathbb{B}} (1 - \Theta_{\mathbb{B}}^o) \left\{ 1 - \frac{1}{2 \ln(\rho)} \left\{ \ln \left[\rho P_a L_{aw}^{o, \mathbb{B}} \left(\frac{\gamma \left(\frac{2}{\nu(\sqrt{2k_{\mathbb{B}})}, [2\rho^o(k_{\mathbb{B}}+1)]^{\frac{\nu(\sqrt{2k_{\mathbb{B}})}}{2}} e^{\mu(\sqrt{2k_{\mathbb{B}})}} \right)}{(k_{\mathbb{B}}+1)\nu(\sqrt{2k_{\mathbb{B}}})e^{\frac{2\mu(\sqrt{2k_{\mathbb{B}}}}{\nu(\sqrt{2k_{\mathbb{B}})}})}} - \rho^o \Theta_{\mathbb{B}}^o \right] + \hat{\sigma}_n^2 \right\} - \ln(\hat{\sigma}_n^2) \right\} \right\}. \quad (30)$$

Lemma 2. If $h_{aw}^{o, \mathbb{B}}$ ($\mathbb{B} \in \{L, N\}$) is the channel fading coefficient of the microwave channel, we have

$$\int_0^a x f_{|h_{aw}^{o, \mathbb{B}}|^2}(x) dx = \frac{\gamma \left(\frac{2}{\nu(\sqrt{2k_{\mathbb{B}})}, [2a(k_{\mathbb{B}}+1)]^{\frac{\nu(\sqrt{2k_{\mathbb{B}})}}{2}} e^{\mu(\sqrt{2k_{\mathbb{B}})}} \right)}{(k_{\mathbb{B}}+1)\nu(\sqrt{2k_{\mathbb{B}}})e^{\frac{2\mu(\sqrt{2k_{\mathbb{B}}}}{\nu(\sqrt{2k_{\mathbb{B}})}})}} - a \exp \left(- [2a(k_{\mathbb{B}}+1)]^{\frac{\nu(\sqrt{2k_{\mathbb{B}})}}{2}} e^{\mu(\sqrt{2k_{\mathbb{B}})}} \right), \quad (27)$$

where $a \geq 0$, $f_{|h_{aw}^{o, \mathbb{B}}|^2}$ is the PDF of $|h_{aw}^{o, \mathbb{B}}|^2$, $\gamma(\cdot, \cdot)$ is the lower incomplete gamma function, $\mu(x)$ and $\nu(x)$ are the polynomial expressions of x as in [50], [51], which are respectively given by

$$\mu(x) \triangleq \begin{cases} -\ln 2, & x = 0, \\ -3.0888 \times 10^{-10} x^6 + 1.8362 \times 10^{-7} x^5 \\ -3.7185 \times 10^{-5} x^4 + 3.4103 \times 10^{-3} x^3 \\ -0.1624 \times x^2 - 1.4318x + 0.7409, & 10 \leq x \leq 8000, \end{cases} \quad (28)$$

$$\nu(x) \triangleq \begin{cases} 2, & x = 0, \\ 5.1546 \times 10^{-11} x^6 - 3.1961 \times 10^{-8} x^5 \\ + 6.3859 \times 10^{-6} x^4 - 5.4159 \times 10^{-4} x^3 \\ + 1.9833 \times 10^{-2} x^2 + 0.9044x + 0.9439, & 10 \leq x \leq 8000. \end{cases} \quad (29)$$

Proof. The detailed proof is presented in Appendix A. ■

Considering the uncertainty of the LoS/NLoS channels, the probability $P_{aw}^{\mathbb{B}}$ should be considered in the calculation of $\mathbb{E}[P_{ew}^{*,o}]$. According to Lemma 2, we can derive $\mathbb{E}[P_{ew}^{*,o}]$ as the following theorem.

Theorem 1. When Alice adopts the OM transmission mode, the expected value $\mathbb{E}[P_{ew}^{*,o}]$ from Alice's perspective is given as (30), where $\rho^o = \frac{(\rho^2-1)\hat{\sigma}_n^2}{\rho P_a L_{aw}^{o, \mathbb{B}}}$ and $\Theta_{\mathbb{B}}^o$ is defined as

$$\Theta_{\mathbb{B}}^o = \exp \left(- [2\rho^o(k_{\mathbb{B}}+1)]^{\frac{\nu(\sqrt{2k_{\mathbb{B}}}}{2}} e^{\mu(\sqrt{2k_{\mathbb{B}})}} \right). \quad (31)$$

Proof. For convenience, let's write $k_1^o = \rho \hat{\sigma}_n^2$ and $k_2^o = k_a^o + \frac{\hat{\sigma}_n^2}{\rho}$. According to (23) in Lemma 1, we have

$$\begin{aligned} \mathbb{E}[P_{ew}^{*,o}] &= \mathbb{E}_{k_1^o < k_2^o} [P_{ew}^{*,o}] \mathbb{P}(k_1^o < k_2^o) + \mathbb{E}_{k_1^o \geq k_2^o} [P_{ew}^{*,o}] \mathbb{P}(k_1^o \geq k_2^o) \\ &= \mathbb{P}(k_1^o \geq k_2^o) \left(1 - \frac{\ln(\rho P_a L_{aw}^{o, \mathbb{B}} \mathbb{E}_{k_1^o \geq k_2^o} [|h_{aw}^{o, \mathbb{B}}|^2] + \hat{\sigma}_n^2) - \ln(\hat{\sigma}_n^2)}{2 \ln(\rho)} \right), \end{aligned} \quad (32)$$

where $\mathbb{P}(k_1^o \geq k_2^o)$ can be derived as

$$\begin{aligned} \mathbb{P}(k_1^o \geq k_2^o) &= \mathbb{P} \left(\rho \hat{\sigma}_n^2 \geq P_a L_{aw}^{o, \mathbb{B}} |h_{aw}^{o, \mathbb{B}}|^2 + \frac{\hat{\sigma}_n^2}{\rho} \right) \\ &= \mathbb{P}(|h_{aw}^{o, \mathbb{B}}|^2 \leq \rho^o) \\ &= 1 - Q_1 \left(\sqrt{2k_{\mathbb{B}}}, \sqrt{2(k_{\mathbb{B}}+1)\rho^o} \right). \end{aligned} \quad (33)$$

To provide some deep analytical insights on the average value of $P_{ew}^{*,o}$, a tight exponential-type approximation for the

standard Marcum-Q function $Q_1(\cdot, \cdot)$ is adopted, which is expressed by

$$Q_1(x, y) \approx \exp(-e^{\mu(x)} y^{\nu(x)}), \quad (34)$$

where $\mu(x)$ and $\nu(y)$ are conditionally defined for $0 \leq x \ll 1$ and $10 \leq x \leq 8000$, which is good range for Rice factors $k_{\mathbb{B}}$ in the concerned system. In this work, we define $\mu(x)$ and $\nu(x)$ as (28) and (29), respectively. The quality and reliability of approximation has been testified where the root mean square error (RMSE) of approximation is less than 0.005 [51]. Thus, we can obtain an approximation of $Q_1(\cdot, \cdot)$ in (33) as

$$\mathbb{P}(k_1^o \geq k_2^o) = 1 - \exp \left(-e^{\mu(\sqrt{2k_{\mathbb{B}}})} [2\rho^o(k_{\mathbb{B}}+1)]^{\frac{\nu(\sqrt{2k_{\mathbb{B}}}}{2}} \right). \quad (35)$$

For the expectation term in (32), we have

$$\begin{aligned} \mathbb{E}_{k_1^o \geq k_2^o} [|h_{aw}^{o, \mathbb{B}}|^2] &= \mathbb{E} \left[|h_{aw}^{o, \mathbb{B}}|^2 \middle| |h_{aw}^{o, \mathbb{B}}|^2 \leq \rho^o \right] \\ &= \int_0^{\rho^o} x f_{|h_{aw}^{o, \mathbb{B}}|^2}(x) dx \\ &\stackrel{(a)}{=} \frac{\gamma \left(\frac{2}{\nu(\sqrt{2k_{\mathbb{B}})}, [2\rho^o(k_{\mathbb{B}}+1)]^{\frac{\nu(\sqrt{2k_{\mathbb{B}}}}{2}} e^{\mu(\sqrt{2k_{\mathbb{B}})}} \right)}{\nu(\sqrt{2k_{\mathbb{B}}})(k_{\mathbb{B}}+1)e^{\frac{2\mu(\sqrt{2k_{\mathbb{B}}}}{\nu(\sqrt{2k_{\mathbb{B}})}}}}} - \rho^o \exp \left(- [2\rho^o(k_{\mathbb{B}}+1)]^{\frac{\nu(\sqrt{2k_{\mathbb{B}}}}{2}} e^{\mu(\sqrt{2k_{\mathbb{B}})}} \right), \end{aligned} \quad (36)$$

where step (a) is due to Lemma 2. Finally, submitting (35) and (36) into (32), we can get $\mathbb{E}[P_{ew}^{*,o}]$ as (30). ■

B. Effective Covert Rate and Covert Shannon Capacity

According to the definition mentioned in Section II-E, the ECR R_{ab}^o can be given as the following theorem.

Theorem 2. When UAV adopts the OM transmission mode in the concerned A2G system, the ECR R_{ab}^o of the system is determined by

$$R_{ab}^o = R_b \times \left\{ 1 - \sum_{\mathbb{B} \in \{L, N\}} P_{ab}^{\mathbb{B}} \left[1 - \mathcal{F}_{\text{Ei}}^o(\rho \hat{\sigma}_n^2) + \mathcal{F}_{\text{Ei}}^o \left(\frac{\hat{\sigma}_n^2}{\rho} \right) \right] \right\}, \quad (37)$$

where R_b is the target rate, $\mathcal{F}_{\text{Ei}}^o(\cdot)$ is defined as following

$$\mathcal{F}_{\text{Ei}}^o(x) = \frac{1}{\nu(\sqrt{2k_{\mathbb{B}}}) \ln \rho} \text{Ei} \left[-e^{\mu(\sqrt{2k_{\mathbb{B}}})} \left(\frac{2(k_{\mathbb{B}}+1)\gamma_{th}x}{P_a L_{ab}^{o, \mathbb{B}}} \right)^{\frac{\nu(\sqrt{2k_{\mathbb{B}}}}{2}} \right], \quad (38)$$

$\mu(x)$ and $\nu(x)$ are defined as (28) and (29) in Theorem 1, respectively, and $\text{Ei}(\cdot)$ is the exponential integral function defined as [52, Eq. (8.211.1)].

Proof. To derive the ECR, we first need to determined the outage probability at Bob P_{out}^o . Considering the uncertainty of the LoS/NLoS channel, the outage probability at Bob P_{out}^o under the OM transmission mode can be determined by

$$P_{out}^o = \sum_{\mathbb{B} \in \{L, N\}} P_{ab}^{\mathbb{B}} \times \mathbb{P}(\gamma_{ab}^o < \gamma_{th}). \quad (39)$$

According to (12), the SNR at Bob is determined by $\gamma_{ab}^o = P_a L_{ab}^{o, \mathbb{B}} |h_{ab}^{o, \mathbb{B}}|^2 / \sigma_b^2$. Thus, the outage probability at Bob P_{out}^o is given by

$$\begin{aligned} \mathbb{P}(\gamma_{ab}^o < \gamma_{th}) &= \mathbb{P}\left(|h_{ab}^{o, \mathbb{B}}|^2 < \frac{\sigma_b^2 \gamma_{th}}{P_a L_{ab}^{o, \mathbb{B}}}\right) \\ &\stackrel{(b)}{=} 1 - \mathbb{E}_{\sigma_b^2} \left[\exp \left(-e^{\mu(\sqrt{2k_{\mathbb{B}}})} \left(\frac{2(k_{\mathbb{B}} + 1) \sigma_b^2 \gamma_{th}}{P_a L_{ab}^{o, \mathbb{B}}} \right)^{\frac{\nu(\sqrt{2k_{\mathbb{B}}})}{2}} \right) \right] \\ &= 1 - \int_{\frac{\sigma_b^2}{\rho}}^{\rho \hat{\sigma}_n^2} \exp \left(-e^{\mu(\sqrt{2k_{\mathbb{B}}})} \left(\frac{2(k_{\mathbb{B}} + 1) \gamma_{th} x}{P_a L_{ab}^{o, \mathbb{B}}} \right)^{\frac{\nu(\sqrt{2k_{\mathbb{B}}})}{2}} \right) \frac{1}{2x \ln \rho} dx \\ &\stackrel{(c)}{=} 1 - \frac{1}{\nu(\sqrt{2k_{\mathbb{B}}}) \ln \rho} \left[\text{Ei} \left(-e^{\mu(\sqrt{2k_{\mathbb{B}}})} \left(\frac{2(k_{\mathbb{B}} + 1) \gamma_{th} x}{P_a L_{ab}^{o, \mathbb{B}}} \right)^{\frac{\nu(\sqrt{2k_{\mathbb{B}}})}{2}} \right) \right]_{\frac{\sigma_b^2}{\rho}}^{\rho \hat{\sigma}_n^2} \\ &= 1 - \frac{1}{\nu(\sqrt{2k_{\mathbb{B}}}) \ln \rho} \text{Ei} \left(-e^{\mu(\sqrt{2k_{\mathbb{B}}})} \left(\frac{2(k_{\mathbb{B}} + 1) \gamma_{th} \rho \hat{\sigma}_n^2}{P_a L_{ab}^{o, \mathbb{B}}} \right)^{\frac{\nu(\sqrt{2k_{\mathbb{B}}})}{2}} \right) \\ &\quad + \frac{1}{\nu(\sqrt{2k_{\mathbb{B}}}) \ln \rho} \text{Ei} \left(-e^{\mu(\sqrt{2k_{\mathbb{B}}})} \left(\frac{2(k_{\mathbb{B}} + 1) \gamma_{th} \sigma_b^2}{P_a L_{ab}^{o, \mathbb{B}}} \right)^{\frac{\nu(\sqrt{2k_{\mathbb{B}}})}{2}} \right), \end{aligned} \quad (40)$$

where step (b) is similar to (35), and step (c) is due to $\int e^{ax^n} x^{-1} dy = \text{Ei}(ax^n)/n$ as [52, Eq. (2.325.7)]. Then, submitting (40) into (39), we can obtain (37). ■

Next, we derive the covert Shannon capacity C_{ab}^o of the concerned system under the OM transmission mode.

Theorem 3. When UAV adopts the OM transmission mode in the concerned A2G system, the CSC C_{ab}^o of the system is determined by

$$C_{ab}^o = \sum_{\mathbb{B} \in \{L, N\}} \frac{W^o P_{ab}^{\mathbb{B}}}{2 \ln 2 \times \ln \rho} \left[\mathcal{F}_{\text{Li}}^o \left(\frac{1}{\rho \hat{\sigma}_n^2} \right) - \mathcal{F}_{\text{Li}} \left(\frac{\rho}{\hat{\sigma}_n^2} \right) \right], \quad (41)$$

where W^o is the bandwidth of microwave, $\mathcal{F}_{\text{Li}}^o(\cdot)$ is given as

$$\mathcal{F}_{\text{Li}}^o(x) = \int_0^\infty \text{Li}_2(-P_a L_{ab}^{o, \mathbb{B}} xy) f_{|h_{ab}^{o, \mathbb{B}}|^2}(y) dy, \quad (42)$$

$\text{Li}_s(\cdot)$ is the polylogarithm of order s , and $f_{|h_{ab}^{o, \mathbb{B}}|^2}(y)$ is refer to (5).

Proof. Considering the possibility of the LoS/NLoS channel, the CSC C_{ab}^o of the A2G system is determined by

$$C_{ab}^o = \sum_{\mathbb{B} \in \{L, N\}} P_{ab}^{\mathbb{B}} \times C_{ab}^o. \quad (43)$$

According to the SNR at Bob, C_{ab}^o can be derived as

$$\begin{aligned} C_{ab}^o &= W^o \mathbb{E}_{|h_{ab}^{o, \mathbb{B}}|^2, \sigma_b^2} \left[\log_2 \left(1 + \frac{P_a L_{ab}^{o, \mathbb{B}} |h_{ab}^{o, \mathbb{B}}|^2}{\sigma_b^2} \right) \right] \\ &= W^o \mathbb{E}_{|h_{ab}^{o, \mathbb{B}}|^2} \left[\frac{1}{2 \ln \rho} \int_{\frac{\sigma_b^2}{\rho}}^{\rho \hat{\sigma}_n^2} \log_2 \left(1 + \frac{P_a L_{ab}^{o, \mathbb{B}} |h_{ab}^{o, \mathbb{B}}|^2}{x} \right) \frac{1}{x} dx \right] \end{aligned}$$

$$\begin{aligned} &= W^o \mathbb{E}_{|h_{ab}^{o, \mathbb{B}}|^2} \left[\frac{1}{2 \ln 2 \ln \rho} \int_{\frac{\sigma_b^2}{\rho}}^{\rho \hat{\sigma}_n^2} \ln \left(1 + P_a L_{ab}^{o, \mathbb{B}} |h_{ab}^{o, \mathbb{B}}|^2 y \right) \frac{1}{y} dy \right] \\ &\stackrel{(c)}{=} W^o \mathbb{E}_{|h_{ab}^{o, \mathbb{B}}|^2} \left[\frac{P_a L_{ab}^{o, \mathbb{B}} |h_{ab}^{o, \mathbb{B}}|^2 y}{2 \ln 2 \ln \rho} [\Phi(-P_a L_{ab}^{o, \mathbb{B}} |h_{ab}^{o, \mathbb{B}}|^2 y, 2, 1)] \right]_{\frac{\sigma_b^2}{\rho}}^{\rho \hat{\sigma}_n^2} \\ &\stackrel{(d)}{=} W^o \mathbb{E}_{|h_{ab}^{o, \mathbb{B}}|^2} \left[\frac{-1}{2 \ln 2 \ln \rho} [\text{Li}_2(-P_a L_{ab}^{o, \mathbb{B}} |h_{ab}^{o, \mathbb{B}}|^2 y)] \right]_{\frac{\sigma_b^2}{\rho}}^{\rho \hat{\sigma}_n^2} \\ &= \frac{W^o}{2 \ln 2 \ln \rho} \int_0^\infty \text{Li}_2 \left(\frac{-P_a L_{ab}^{o, \mathbb{B}} x}{\rho \hat{\sigma}_n^2} \right) f_{|h_{ab}^{o, \mathbb{B}}|^2}(x) dx \\ &\quad - \frac{W^o}{2 \ln 2 \ln \rho} \int_0^\infty \text{Li}_2 \left(\frac{-\rho P_a L_{ab}^{o, \mathbb{B}} x}{\hat{\sigma}_n^2} \right) f_{|h_{ab}^{o, \mathbb{B}}|^2}(x) dx, \end{aligned} \quad (44)$$

where step (c) is according to [52, Eq. (2.728.2)], $\Phi(\cdot, \cdot, \cdot)$ is Lerch function defined as [52, Eq. (9.550)], and step (d) is due to $\text{Li}_s(z) = z \Phi(z, s, 1)$. Submitting (44) into (43), we can obtain (41). ■

V. COVERT PERFORMANCE ANALYSIS UNDER THE DM TRANSMISSION MODE

Similar to Section IV, this section investigates the optimal detection threshold and the corresponding minimum DEP at Willie, as well as the expected minimum DEP from Alice's perspective, lastly, the ECR and CSC under the DM transmission mode.

A. Detection Error Probability

According to (16) and (18), when Alice does not transmit information, Willie only received the background noise. Thus, P_{FA}^d is same as (20). While Alice transmits information, by observing the equation deducing in (21), we can obtain P_{MD}^d by replacing the parameter k_a^o in (21) with $k_a^d = P_a G_{aw} L_{aw}^{d, \mathbb{B}} |h_{aw}^{d, \mathbb{B}}|^2$. Based on P_{FA}^d and P_{MD}^d , we can further derive the optimal detection threshold and the minimum detection error probability at Willie as the following lemma.

Lemma 3. When Alice adopts the DM transmission mode, the optimal detection threshold τ^* for Willie's detector is in the interval

$$\tau^* \in \begin{cases} [\rho \hat{\sigma}_n^2, k_a^d + \frac{\hat{\sigma}_n^2}{\rho}], & \rho \hat{\sigma}_n^2 < k_a^d + \frac{\hat{\sigma}_n^2}{\rho}, \\ k_a^d + \frac{\hat{\sigma}_n^2}{\rho}, & \rho \hat{\sigma}_n^2 \geq k_a^d + \frac{\hat{\sigma}_n^2}{\rho}, \end{cases} \quad (45)$$

and the corresponding minimum DEP $P_{ew}^{*,d}$ is given as

$$P_{ew}^{*,d} = \begin{cases} 0, & \rho \hat{\sigma}_n^2 < k_a^d + \frac{\hat{\sigma}_n^2}{\rho}, \\ 1 - \frac{\ln(\rho k_a^d + \hat{\sigma}_n^2) - \ln(\hat{\sigma}_n^2)}{2 \ln \rho}, & \rho \hat{\sigma}_n^2 \geq k_a^d + \frac{\hat{\sigma}_n^2}{\rho}, \end{cases} \quad (46)$$

where $k_a^d = P_a G_{aw} L_{aw}^{d, \mathbb{B}} |h_{aw}^{d, \mathbb{B}}|^2$, ρ and $\hat{\sigma}_n^2$ are the parameter that quantifies the size of the uncertainty and nominal noise power, respectively, which are defined in Section II-D.

Proof. The proof is similar to Lemma 1, we omit it here. ■

Similar to Theorem 1, Alice and Bob only rely on the expected measure of $P_{ew}^{*,d}$ to evaluate the covertness under the DM mode. Note that $\mathbb{E}[P_{ew}^{*,d}]$ is related with the numerical integration of $|h_{aw}^{m, \mathbb{B}}|^2$. Thus before deriving $\mathbb{E}[P_{ew}^{*,d}]$, we first present the following lemma.

$$\mathbb{E}[P_{ew}^{*,d}] = \sum_{\mathbb{A} \in \{M,S\}} P_{\mathbb{A}}^{\mathbb{A}} \sum_{\mathbb{B} \in \{L,N\}} P_{\mathbb{B}}^{\mathbb{B}} (1 + \Theta_{\mathbb{B}}^d) \left\{ 1 - \frac{1}{2 \ln \rho} \left[\ln \left[\rho P_{\mathbb{A}} G_{\mathbb{A}}^{\mathbb{A}} G_{\mathbb{B}}^{\mathbb{B}} L_{\mathbb{A}\mathbb{B}}^{m,\mathbb{B}} \left(\varrho^d \Theta_{\mathbb{B}}^d - \sum_{r=1}^{S_{\mathbb{B}}} \binom{S_{\mathbb{B}}}{r} (-1)^r \frac{1 - e^{-r \xi_{\mathbb{B}} \varrho^d}}{r \xi_{\mathbb{B}}} \right) + \hat{\sigma}_n^2 \right] - \ln(\hat{\sigma}_n^2) \right] \right\}. \quad (48)$$

Lemma 4. If $h_{aw}^{m,\mathbb{B}}$ ($\mathbb{B} \in \{L,N\}$) is the channel fading coefficient of the mmWave channel, we have

$$\int_0^a x f_{|h_{aw}^{m,\mathbb{B}}|^2}(x) dx = \sum_{r=1}^{S_{\mathbb{B}}} \binom{S_{\mathbb{B}}}{r} (-1)^r \left[a e^{-r \xi_{\mathbb{B}} a} - \frac{1 - e^{-r \xi_{\mathbb{B}} a}}{r \xi_{\mathbb{B}}} \right], \quad (47)$$

where $f_{|h_{aw}^{m,\mathbb{B}}|^2}$ is the PDF of $|h_{aw}^{m,\mathbb{B}}|^2$.

Proof. The detailed proof is presented in Appendix B. ■

Note that the probability of channel model uncertainty as well as antenna gain uncertainty needs to be considered simultaneously. Thus, when UAV adopts the DM transmission mode, $\mathbb{E}[P_{ew}^{*,d}]$ can be given as follows.

Theorem 4. When Alice adopts the DM transmission mode, the expected value $\mathbb{E}[P_{ew}^{*,d}]$ from Alice's perspective is given as (48), where $G_{\mathbb{A}}^{\mathbb{A}}$ is refer to (1), $\varrho^d = \frac{(\rho^2 - 1)\hat{\sigma}_n^2}{\rho P_{\mathbb{A}} G_{\mathbb{A}}^{\mathbb{A}} G_{\mathbb{B}}^{\mathbb{B}} L_{\mathbb{A}\mathbb{B}}^{m,\mathbb{B}}}$, and $\Theta_{\mathbb{B}}^d$ is defined as

$$\Theta_{\mathbb{B}}^d = \sum_{r=1}^{S_{\mathbb{B}}} \binom{S_{\mathbb{B}}}{r} (-1)^r e^{-r \xi_{\mathbb{B}} \varrho^d}. \quad (49)$$

Proof. For convenience, let's denote $k_1^d = \rho \hat{\sigma}_n^2$ and $k_2^d = k_a^d + \frac{\hat{\sigma}_n^2}{\rho}$. According to (46) in Lemma 3, we have

$$\begin{aligned} \mathbb{E}[P_{ew}^{*,d}] &= \mathbb{E}_{k_1^d < k_2^d} [P_{ew}^{*,d}] \mathbb{P}(k_1^d < k_2^d) + \mathbb{E}_{k_1^d \geq k_2^d} [P_{ew}^{*,d}] \mathbb{P}(k_1^d \geq k_2^d) \\ &= \mathbb{P}(k_1^d \geq k_2^d) \\ &\quad \times \left(1 - \frac{\ln(\rho P_{\mathbb{A}} G_{\mathbb{A}}^{\mathbb{A}} G_{\mathbb{B}}^{\mathbb{B}} L_{\mathbb{A}\mathbb{B}}^{m,\mathbb{B}} \mathbb{E}_{k_1^d \geq k_2^d} [|h_{aw}^{m,\mathbb{B}}|^2] + \hat{\sigma}_n^2) - \ln(\hat{\sigma}_n^2)}{2 \ln(\rho)} \right), \end{aligned} \quad (50)$$

where the term $\mathbb{P}(k_1^d \geq k_2^d)$, we can get

$$\begin{aligned} \mathbb{P}(k_1^d \geq k_2^d) &= \mathbb{P}\left(\rho \hat{\sigma}_n^2 \geq P_{\mathbb{A}} G_{\mathbb{A}}^{\mathbb{A}} G_{\mathbb{B}}^{\mathbb{B}} L_{\mathbb{A}\mathbb{B}}^{m,\mathbb{B}} |h_{aw}^{m,\mathbb{B}}|^2 + \frac{\hat{\sigma}_n^2}{\rho}\right) \\ &= \mathbb{P}(|h_{aw}^{m,\mathbb{B}}|^2 \leq \varrho^d) = \sum_{r=0}^{S_{\mathbb{B}}} \binom{S_{\mathbb{B}}}{r} (-1)^r e^{-r \xi_{\mathbb{B}} \varrho^d}. \end{aligned} \quad (51)$$

For the expectation term in (50), we have

$$\begin{aligned} \mathbb{E}_{k_1^d \geq k_2^d} [|h_{aw}^{m,\mathbb{B}}|^2] &= \mathbb{E} \left[|h_{aw}^{m,\mathbb{B}}|^2 \middle| |h_{aw}^{m,\mathbb{B}}|^2 \leq \varrho^d \right] \\ &= \int_0^{\varrho^d} x f_{|h_{aw}^{m,\mathbb{B}}|^2}(x) dx \\ &\stackrel{(a)}{=} \sum_{r=1}^{S_{\mathbb{B}}} \binom{S_{\mathbb{B}}}{r} (-1)^r \left[\varrho^d e^{-r \xi_{\mathbb{B}} \varrho^d} - \frac{1 - e^{-r \xi_{\mathbb{B}} \varrho^d}}{r \xi_{\mathbb{B}}} \right], \end{aligned} \quad (52)$$

where step (a) is due to Lemma 4. Finally, substituting (51), (52) into (50), we can obtain $\mathbb{E}[P_{ew}^{*,d}]$ as (48). ■

B. Effective Covert Rate and Covert Shannon Capacity

Similarly as in Section IV-B, the ECR R_{ab}^d of the system under the DM transmission mode can be given as the following theorem.

Theorem 5. When UAV adopts the DM transmission mode, the ECR R_{ab}^d of the concerned A2G system is given by

$$R_{ab}^d = R_b \times \left\{ 1 - \sum_{\mathbb{A} \in \{M,S\}} P_{\mathbb{A}}^{\mathbb{A}} \sum_{\mathbb{B} \in \{L,N\}} P_{\mathbb{B}}^{\mathbb{B}} \left[1 + \mathcal{F}_{\text{Ei}}^d(\rho \hat{\sigma}_n^2) - \mathcal{F}_{\text{Ei}}^d\left(\frac{\hat{\sigma}_n^2}{\rho}\right) \right] \right\}, \quad (53)$$

where R_b is the target covert rate, and $\mathcal{F}_{\text{Ei}}^d(\cdot)$ in (53) is defined as following

$$\mathcal{F}_{\text{Ei}}^d(x) = \sum_{r=1}^{S_{\mathbb{B}}} \binom{S_{\mathbb{B}}}{r} (-1)^r \frac{1}{2 \ln \rho} \text{Ei} \left(\frac{-r \xi_{\mathbb{B}} \gamma_{th} x}{P_{\mathbb{A}} G_{\mathbb{A}}^{\mathbb{A}} G_{\mathbb{B}}^{\mathbb{B}} L_{\mathbb{A}\mathbb{B}}^{m,\mathbb{B}}} \right). \quad (54)$$

Proof. Similarly, to analyze the ECR, we need to determine the outage probability P_{out}^d at Bob. Due to the uncertainties of the LoS/NLoS channel and antenna gains, the outage probability at Bob P_{out}^d under the DM transmission mode can be determined by

$$P_{out}^d = \sum_{\mathbb{A} \in \{M,S\}} P_{\mathbb{A}}^{\mathbb{A}} \sum_{\mathbb{B} \in \{L,N\}} P_{\mathbb{B}}^{\mathbb{B}} \times \mathbb{P}(\gamma_{ab}^d < \gamma_{th}). \quad (55)$$

According to (14), the SNR at Bob is given as $\gamma_{ab}^d = P_{\mathbb{A}} G_{\mathbb{A}}^{\mathbb{A}} L_{\mathbb{A}\mathbb{B}}^{d,\mathbb{B}} |h_{ab}^{d,\mathbb{B}}|^2 / \sigma_b^2$. Thus, the outage probability at Bob P_{out}^d is given by

$$\begin{aligned} \mathbb{P}(\gamma_{ab}^d < \gamma_{th}) &= \mathbb{P} \left(\frac{P_{\mathbb{A}} G_{\mathbb{A}}^{\mathbb{A}} G_{\mathbb{B}}^{\mathbb{B}} L_{\mathbb{A}\mathbb{B}}^{m,\mathbb{B}} |h_{ab}^{m,\mathbb{B}}|^2}{\sigma_b^2} < \gamma_{th} \right) \\ &= \mathbb{P} \left(|h_{ab}^{m,\mathbb{B}}|^2 < \frac{\sigma_b^2 \gamma_{th}}{P_{\mathbb{A}} G_{\mathbb{A}}^{\mathbb{A}} G_{\mathbb{B}}^{\mathbb{B}} L_{\mathbb{A}\mathbb{B}}^{m,\mathbb{B}}} \right) \\ &= \sum_{r=0}^{S_{\mathbb{B}}} \binom{S_{\mathbb{B}}}{r} (-1)^r \mathbb{E}_{\sigma_b^2} \left[\exp \left(\frac{-r \xi_{\mathbb{B}} \gamma_{th} \sigma_b^2}{P_{\mathbb{A}} G_{\mathbb{A}}^{\mathbb{A}} G_{\mathbb{B}}^{\mathbb{B}} L_{\mathbb{A}\mathbb{B}}^{m,\mathbb{B}}} \right) \right] \\ &= 1 + \sum_{r=1}^{S_{\mathbb{B}}} \binom{S_{\mathbb{B}}}{r} (-1)^r \int_{\frac{\sigma_b^2}{\rho}}^{\rho \hat{\sigma}_n^2} \exp \left(\frac{-r \xi_{\mathbb{B}} \gamma_{th} x}{P_{\mathbb{A}} G_{\mathbb{A}}^{\mathbb{A}} G_{\mathbb{B}}^{\mathbb{B}} L_{\mathbb{A}\mathbb{B}}^{m,\mathbb{B}}} \right) \frac{1}{2x \ln \rho} dx \\ &\stackrel{(a)}{=} 1 + \sum_{r=1}^{S_{\mathbb{B}}} \binom{S_{\mathbb{B}}}{r} (-1)^r \frac{1}{2 \ln \rho} \text{Ei} \left(\frac{-r \xi_{\mathbb{B}} \gamma_{th} x}{P_{\mathbb{A}} G_{\mathbb{A}}^{\mathbb{A}} G_{\mathbb{B}}^{\mathbb{B}} L_{\mathbb{A}\mathbb{B}}^{m,\mathbb{B}}} \right) \Big|_{\frac{\sigma_b^2}{\rho}}^{\rho \hat{\sigma}_n^2} \\ &= 1 + \sum_{r=1}^{S_{\mathbb{B}}} \binom{S_{\mathbb{B}}}{r} (-1)^r \frac{1}{2 \ln \rho} \text{Ei} \left(\frac{-r \xi_{\mathbb{B}} \gamma_{th} \rho \hat{\sigma}_n^2}{P_{\mathbb{A}} G_{\mathbb{A}}^{\mathbb{A}} G_{\mathbb{B}}^{\mathbb{B}} L_{\mathbb{A}\mathbb{B}}^{m,\mathbb{B}}} \right) \\ &\quad - \sum_{r=1}^{S_{\mathbb{B}}} \binom{S_{\mathbb{B}}}{r} (-1)^r \frac{1}{2 \ln \rho} \text{Ei} \left(\frac{-r \xi_{\mathbb{B}} \gamma_{th} \hat{\sigma}_n^2}{P_{\mathbb{A}} G_{\mathbb{A}}^{\mathbb{A}} G_{\mathbb{B}}^{\mathbb{B}} L_{\mathbb{A}\mathbb{B}}^{m,\mathbb{B}}} \right), \end{aligned} \quad (56)$$

where step (a) is due to $\int e^{ax} x^{-1} dy = \text{Ei}(ax)$ [52, Eq. (2.325.1)]. Then, submitting (56) into (55), we obtain (53). ■

Next, we derive the covert Shannon capacity C_{ab}^d of the considered system under the DM transmission mode.

Theorem 6. *In the considered A2G system, the CSC C_{ab}^d of the system under the DM transmission mode is determined by*

$$C_{ab}^d = \sum_{\mathbb{A} \in \{M, S\}} P_b^{\mathbb{A}} \sum_{\mathbb{B} \in \{L, N\}} P_{ab}^{\mathbb{B}} \frac{W^d}{2 \ln 2 \times \ln \rho} \left[\mathcal{F}_{\text{Li}}^d \left(\frac{1}{\rho \hat{\sigma}_n^2} \right) - \mathcal{F}_{\text{Li}}^d \left(\frac{\rho}{\hat{\sigma}_n^2} \right) \right], \quad (57)$$

where W^d is the bandwidth of mmWave, and $\mathcal{F}_{\text{Li}}^d(\cdot)$ in (57) is defined as following

$$\mathcal{F}_{\text{Li}}^d(x) = \int_0^\infty \text{Li}_2(-P_a G_a^M G_b^{\mathbb{A}} L_{ab}^{m, \mathbb{B}} xy) f_{|h_{ab}^{m, \mathbb{B}}|^2}(y) dy, \quad (58)$$

$\text{Li}_2(\cdot)$ is refer to Theorem 3, and $f_{|h_{ab}^{m, \mathbb{B}}|^2}(y)$ is refer to (8).

Proof. The proof is similar to Theorem 3, we omit here. ■

VI. PERFORMANCE OPTIMIZATION AND MODE SELECTION

In this section, we establish the optimization problems of the ECR and CSC maximization under the OM and DM transmission modes, and further propose a hybrid OM/DM transmission mode.

A. Maximum Effective Covert Rate

From Theorem 2 and 5, we note that the ECR R_{ab} is related with the transmission power P_a and target rate R_b . Besides, a large P_a and R_b results in a small $\mathbb{E}[P_{ew}^{*, \mathbb{C}}]$ and a large P_{out} , respectively. Thus, for a certain position $U(x, y, z)$, the UAV intends to find its optimal transmission power P_a and optimal target rate R_b to maximize R_{ab} with the DEP constraint. The corresponding optimal problems under the OM and DM transmission modes can be respectively formulated as the follows

$$\bar{R}_{a,b}^{*,o}(x_a, y_a, h_a) = \max_{P_a, R_b} R_{ab}^o(x_a, y_a, h_a), \quad (59a)$$

$$s.t. \quad \mathbb{E}[P_{ew}^{*, \mathbb{C}}] \geq 1 - \epsilon \quad (59b)$$

$$P_a \leq P_{max} \quad (59c)$$

and

$$\bar{R}_{a,b}^{*,d}(x_a, y_a, h_a) = \max_{P_a, R_b} R_{ab}^d(x_a, y_a, h_a), \quad (60a)$$

$$s.t. \quad \mathbb{E}[P_{ew}^{*, \mathbb{C}}] \geq 1 - \epsilon \quad (60b)$$

$$P_a \leq P_{max} \quad (60c)$$

where $\bar{R}_{a,b}^{*,o}(x, y, h_a)$ (resp. $\bar{R}_{a,b}^{*,d}(x, y, h_a)$) denotes the maximum $R_{ab}^o(x, y, h_a)$ (resp. $R_{ab}^d(x, y, h_a)$), which characterizes the maximum of average *successfully* transmitted amount of information subject to a covertness requirement ϵ . Although we cannot obtain a closed-form result of optimal transmission power and optimal target rate due to transcendental functions, we can obtain the optimal solutions by numerical search methods.

B. Maximum Covert Shannon Capacity

According to Theorem 3 and 6, we know that a larger P_a will lead to a larger CSC C_{ab} . But, according to the detection strategy of Willie, a large P_a also lead to a lower DEP $\mathbb{E}[P_{ew}^{*, \mathbb{C}}]$. Therefore, UAV hopes to maximize the CSC of the A2G system by optimizing the transmission power under the OM and DM transmission modes, which can be respectively formulated as

$$\bar{C}_{a,b}^{*,o}(x_a, y_a, h_a) = \max_{P_a} C_{ab}^o(x_a, y_a, h_a), \quad (61a)$$

$$s.t. \quad \mathbb{E}[P_{ew}^{*, \mathbb{C}}] \geq 1 - \epsilon \quad (61b)$$

$$P_a \leq P_{max} \quad (61c)$$

and

$$\bar{C}_{a,b}^{*,d}(x_a, y_a, h_a) = \max_{P_a} C_{ab}^d(x_a, y_a, h_a), \quad (62a)$$

$$s.t. \quad \mathbb{E}[P_{ew}^{*, \mathbb{C}}] \geq 1 - \epsilon \quad (62b)$$

$$P_a \leq P_{max} \quad (62c)$$

where $\bar{C}_{a,b}^{*,o}(x_a, y_a, h_a)$ (resp. $\bar{C}_{a,b}^{*,d}(x_a, y_a, h_a)$) denote the maximum $C_{ab}^o(x_a, y_a, h_a)$ (resp. $C_{ab}^d(x_a, y_a, h_a)$), which characterizes the *upper bound* of the time average rate of messages delivered from transmitter to the destination subject to a covertness requirement ϵ . Similarly, we can solve these optimization problems through numerical search methods.

C. Optimal Transmission Mode for Covert Communication

Although mmWave has a larger bandwidth than low-frequency microwave, it also have the disadvantage of faster attenuation. Thus, with the dynamic change of the distance from UAV to Bob and Willie, respectively, the hybrid OM/DM transmission mode of the UAV would be superior to the pure OM or DM transmission mode in terms of covert performance. To confirm our idea, we propose a hybrid OM/DM transmission mode which allows UAV to adaptively switch between the OM and DM transmission modes based on (59)-(62). Specifically, for a given position (x_a, y_a, h_a) of UAV, we first calculate the distance d_{ab} from UAV to Bob and the distance d_{aw} from UAV to Willie. Then, we submit them into (59) and (60) (resp. (61) and (61)) and solve the optimal problems. We select the optimal transmission mode I_{ECR} (resp. I_{CSC}) by comparing $\bar{R}_{a,b}^{*,o}(x_a, y_a, h_a)$ and $\bar{R}_{a,b}^{*,d}(x_a, y_a, h_a)$ (resp. $\bar{C}_{a,b}^{*,o}(x_a, y_a, h_a)$ and $\bar{C}_{a,b}^{*,d}(x, y, z)$), where I_{ECR} and I_{CSC} are the indicators of the optimal selection mode for maximizing the ECR and CSC, which are respectively denoted as

$$I_{ECR} = \begin{cases} \text{OM mode,} & \bar{R}_{a,b}^{*,o}(x_a, y_a, h_a) \geq \bar{R}_{a,b}^{*,d}(x_a, y_a, h_a), \\ \text{DM mode,} & \text{otherwise,} \end{cases} \quad (63)$$

and

$$I_{CSC} = \begin{cases} \text{OM mode,} & \bar{C}_{a,b}^{*,o}(x_a, y_a, h_a) \geq \bar{C}_{a,b}^{*,d}(x_a, y_a, h_a), \\ \text{DM mode,} & \text{otherwise.} \end{cases} \quad (64)$$

Overall, the hybrid OM/DM transmission mode selection algorithm for optimal covert communication can be described as Algorithm 1.

Algorithm 1: Hybrid OM/DM Transmission Mode Selection Algorithm

input : UAV's location $U(x_a, y_a, h_a)$, Bob's location $U(x_b, y_b, h_b)$, Willie's location $U(x_w, y_w, h_w)$.

output: The mode selection indicator I_{ECR} or I_{CSC} .

- 1 Calculate the distances d_{ab} and d_{aw} , respectively.
 - 2 **if** UAV intends to maximize the ECR **then**
 - 3 Submit d_{ab} and d_{aw} into (59) and (60) and solve the optimal problems;
 - 4 Obtain I_{ECR} by comparing $\bar{R}_{ab}^{*,o}(x_a, y_a, h_a)$ with $\bar{R}_{ab}^{*,d}(x_a, y_a, h_a)$ according to (63).
 - 5 **else if** UAV intends to maximize the CSC **then**
 - 6 Submit d_{ab} and d_{aw} into (61) and (62) and solve the optimal problems;
 - 7 Obtain I_{CSC} by comparing $\bar{C}_{ab}^{*,o}(x_a, y_a, h_a)$ with $\bar{C}_{ab}^{*,d}(x_a, y_a, h_a)$ according to (64).
 - 8 **end**
 - 9 **Return** I_{ECR} or I_{CSC} .
-

TABLE II
NETWORK PARAMETER SETTINGS

Network Parameters	Values
UPA antenna elements ($\mathcal{N}_a, \mathcal{N}_b, \mathcal{N}_w$)	(6, 18, 18)
S-curve parameters (σ, f)	(4.88, 0.429)
OM channel path loss coefficients (β_L^o, β_N^o)	($10^{-6}, 10^{-7}$)
OM channel path loss exponents (α_L^o, α_N^o)	(1.64, 2.71)
DM channel path loss coefficients (β_L^d, β_N^d)	($10^{-6.11}, 10^{-7.18}$)
DM channel path loss exponents (α_L^d, α_N^d)	(2, 3)
Rician factor ($k_0, k_{\pi/2}$)	(5, 15) dBm
Nakagami-m fading shape parameters (S_L, S_N)	(3, 2)
Nominal noise power $\hat{\sigma}_n^2$	-80 dBm
Noise uncertainty level ρ	2 dB
Target rate R_b	1 Mbits/s/Hz
Covertess requirement ϵ	0.2

VII. NUMERICAL RESULTS

This section provides extensive numerical results to illustrate the system performance under both the OM mode and DM mode, such that optimal model for covert communication in the concerned hybrid microwave/mmWave A2G systems can be obtained.

In the following, we considered the A2G system where Bob is located at $(-500, 0, 0)$, Willie is located at $(1000, 0, 0)$, UAV flies at a fixed altitude of $h_a = 500\text{m}$, the minimum and maximum safe distance limits for UAV flight are $d_{aw}^{min} = 300\text{m}$ and $d_{aw}^{max} = 1500\text{m}$, respectively. The OM transmission mode of Alice transmits at a typical frequency 2.5GHz with 40-MHz bandwidth as [53], and the DM transmission mode transmits at a typical mmWave frequency 73GHz and with 100-MHz bandwidth as [32], [54]. We summarized the considered parameters in Table II, unless explicitly mentioned.

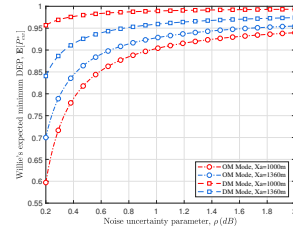


Fig. 2. The expected minimum DEP $\mathbb{E}[P_{ew}^*]$ vs. noise uncertainty ρ .

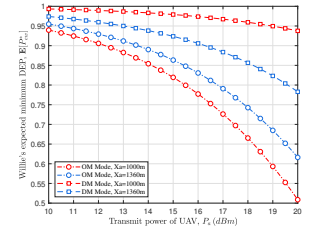


Fig. 3. The expected minimum DEP $\mathbb{E}[P_{ew}^*]$ vs. transmission power P_a .

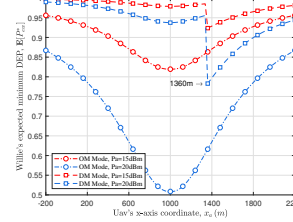


Fig. 4. The expected minimum DEP $\mathbb{E}[P_{ew}^*]$ vs. horizontal position x_a .

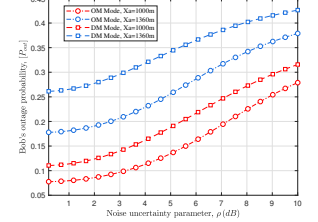


Fig. 5. Outage probability P_{out} vs. noise uncertainty parameter ρ .

A. Analysis of Expected Minimum DEP

We first explore the impact of parameter ρ which is used to quantify the level of the noise uncertainty on the expected minimum DEP $\mathbb{E}[P_{ew}^*]$ at Willie. As depicted in Fig. 2, $\mathbb{E}[P_{ew}^*]$ keeps increasing as ρ increases. This is because the greater the level of noise uncertainty, the more conducive to hide the message transmission of Alice. We also can observe that, for a given position of Alice, i.e., $x_a = 1000\text{m}$ and $x_a = 1360\text{m}$, the DM transmission mode is superior to the OM transmission mode in terms of covert performance. Due to the fast fading characteristic of mmWave, the probability of misjudgment under the DM mode is higher than that in the OM mode. From Fig. 2, we can further observe that, for the DM transmission mode, $\mathbb{E}[P_{ew}^*]$ of Willie is higher when $x_a = 1000\text{m}$ than that one when $x_a = 1360\text{m}$, which is opposite of the OM transmission mode. The reason behind the phenomena can be explained that, Alice always steers her main lobe of the DM antenna to Bob, when $x_a = 1360\text{m}$, Willie is also located in the boresight direction of the main lobe, such that he can obtain more power from Alice, thereby reducing $\mathbb{E}[P_{ew}^*]$.

We then investigate the impact of the transmission power of Alice P_a on the expected minimum DEP $\mathbb{E}[P_{ew}^*]$ with $\rho = 2\text{dB}$ and $x_a = \{1000\text{m}, 1360\text{m}\}$. As shown in Fig. 3, it can be observed that $\mathbb{E}[P_{ew}^*]$ is monotonically decreasing with respect to P_a . That is because as the transmission power increases, it is not conducive to hiding the information in the background noise. Also, as P_a increases, the expected minimum DEP performance in OM transmission mode degrades faster than in DM transmission mode. Because the mmWave attenuates faster than the microwave, and the received power at Willie remains lower under the same transmission power.

To explore the impact of the position of Alice x_a on the expected minimum DEP $\mathbb{E}[P_{ew}^*]$, we summarize in Fig. 4 to show how $\mathbb{E}[P_{ew}^*]$ varies with x_a with $P_a = \{15\text{dBm}, 20\text{dBm}\}$. From Fig. 4, we can see that $\mathbb{E}[P_{ew}^*]$ first decreases as x_a increases from -200m to 1000m , and then increases after 1000m under the OM transmission mode. It is due to the fact that Alice just moves right above Willie, the distance between

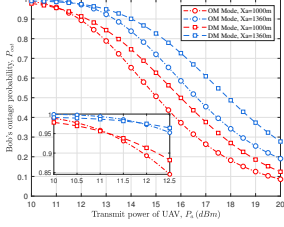


Fig. 6. Outage probability P_{out} vs. transmission power P_a .

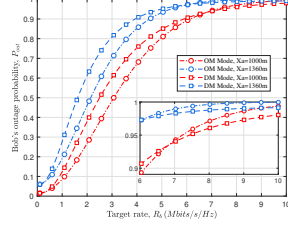


Fig. 7. Outage probability P_{out} vs. target rate R_b .

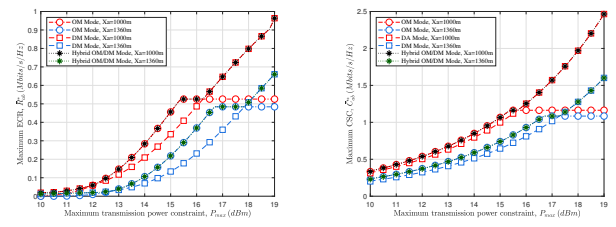
them is the closest, and Willie can detect the transmission behavior of Alice more accurately. For the DM transmission mode, we can see that when $x_a = 1360m$, $\mathbb{E}[P_{ew}^*]$ decreases sharply to the minimal value and then gradually increase as x_a increases. This interesting phenomenon can be explained as when $x_a = 1360m$, Willie is just in the half-power beam width direction of the antenna array of link Alice \rightarrow Bob and he can obtain more power benefiting from the main lobe antenna gain of Alice. But as x_a increases, the distance between Willie and Alice will increase and the received power at Willie will decrease causing an increasing $\mathbb{E}[P_{ew}^*]$.

B. Analysis of Outage Probability

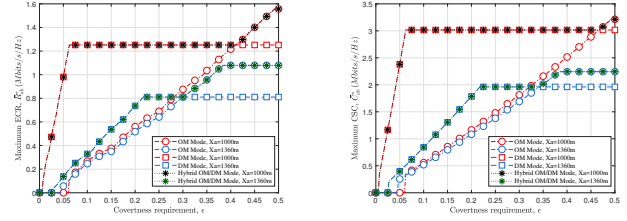
We plot Fig. 5 to explore the impact of noise uncertainty parameter ρ on the outage probability P_{out} under both the OM and DM transmission modes. From Fig. 5, we can see that as ρ increases, P_{out} gradually increases. A larger ρ leads to a lower SNR at Bob such that the outage probability is higher. Note that we also can find that under a given x_a and ρ , the OM transmission mode outperforms the DM transmission mode in terms of the outage probability performance. This phenomenon can be attributed to the fast fading of mmWave resulting in a small SNR at Bob.

Fig. 6 is used to study the impact of transmission power P_a on the outage probability P_{out} . We can see from Fig. 6 that the outage probability P_{out} monotonically decreases with respect to P_a . Obviously, a larger P_a will lead to a higher SNR resulting in a lower outage probability. A further careful observation of Fig. 6 indicates that when Alice transmits with a small P_a , P_{out} under the OM transmission mode is higher than the one under the DM transmission mode, but once P_a exceeds a certain value, P_{out} under the OM transmission mode is lower than the one under the DM transmission mode. Note that when Alice transmits with a lower power, mmWave directional antenna can offset a tiny part of channel fading. Thus, the outage probability under the DM transmission mode is lower than that one under the OM transmission mode. But, the channel fading of mmWave is much faster than the microwave, such that when Alice transmits with a big power, the received power of Bob under the DM transmission mode than the one under the OM transmission mode, resulting in a higher outage probability.

To further study the changing trend of the outage probability P_{out} varying with the target rate R_b under both transmission modes, we draw Fig. 7. We can observe that as the target rate R_b increases, the outage probability P_{out} also increases. It can be easily explained based on the definition of the



(a) ECR \bar{R}_{ab}^* (b) CSC \bar{C}_{ab}^*
Fig. 8. Covert performance vs. maximum transmission power constraint P_{max} with $x_a \in \{1000m, 1360m\}$.



(a) ECR \bar{R}_{ab}^* (b) CSC \bar{C}_{ab}^*
Fig. 9. Covert performance vs. covertness constraint ϵ with $x_a \in \{1000m, 1360m\}$ and $P_{max} = 20dBm$.

outage probability. Besides, it also implies that there is a trade-off relationship between P_{out} and R_b which validates the rationality of optimizing R_b in this work.

C. Analysis of ECR and CSC

To explore the impact of the maximum power constraint P_{max} on the maximum ECR \bar{R}_{ab}^* and CSC \bar{C}_{ab}^* under both two modes, we summarize in Fig. 8 how they vary with P_{max} with $x_a = 1000m$ and $x_a = 1360m$, respectively. From Fig. 8(a), we can see that as P_{max} increases, \bar{R}_{ab}^* gradually increases and then tends to a constant under the OM transmission mode. It can be explained as that a larger P_{max} can allow Alice uses more power to transmit information resulting in a smaller P_{out} . But the covert performance constraint limits that P_a cannot increase all the time. Thus, when P_{max} is enough large, \bar{R}_{ab}^* reaches its maximum value and keeps constant. For the DM transmission mode, due to the fast fading of mmWave, even given a large P_{max} , the received power at Willie is still small and the DEP is still high. Thus, Alice can still increase P_a to improve the effective covert rate. The corresponding analysis can be applied to illustrate the phenomenon of the covert capacity \bar{C}_{ab}^* in Fig. 8(b), we omit here.

We then investigate the impact of the covertness constraint ϵ on the maximum effective covert rate \bar{R}_{ab}^* and covert capacity \bar{C}_{ab}^* . The results are summarized in Fig. 9. We can observe from Fig. 9 that as ϵ increases, both \bar{R}_{ab}^* and \bar{C}_{ab}^* first increase and then tends to remain unchanged. This can be explained as follows. As the covert constraints are gradually relaxed, Alice can adopt a large P_a to transmit the covert information and thus both \bar{R}_{ab}^* and \bar{C}_{ab}^* increase. But when P_a is large enough, the transmission power remains unchanged due to the maximum power constraint P_{max} . We further observe from Fig. 9(a) and Fig. 9(b) that under the hybrid mode, adopting the OM transmission mode can achieve better performance when the covertness restrictions are relaxed enough, while

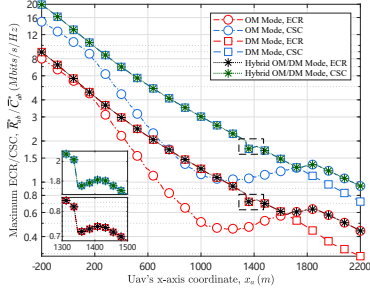


Fig. 10. Covert performance vs. horizontal position of UAV x_a .

adopting the DM transmission mode is better when the covert-ness constraint is strict.

Finally, we investigate the performance of different x_a during the movement of Alice. We summarized in Fig. 10 how the covert performance varies with x_a for a setting of $\rho = 2\text{dB}$ and $P_{\max} = 20\text{dBm}$. We can see from Fig. 10 that during Alice's movement from $(-200, 0, 500)$ to $(2200, 0, 500)$, the covert performance first decreases and then increases and finally decreases under both transmission modes. The interesting behavior can be explained as follows. When Alice moves away from Bob and closes to Willie, due to the negative effects brought by the path attenuation and covert constraint, both R_{ab}^* and C_{ab}^* will decrease quickly. When Alice moves away from Willie, the power received by Willie decreases, and it can increase P_a appropriately to improve the transmission efficiency. When Alice moves far away from Willie and Bob enough, Alice can adopt a larger transmission power satisfying the covertness constraint, however, it cannot offset the negative impact of large-scale attenuation on transmission performance. Thus, both \bar{R}_{ab}^* and \bar{C}_{ab}^* will decrease. Moreover, from Fig 10, we can see that when Alice is far away from Willie, the DM transmission mode outperforms the OM transmission mode in terms of both \bar{R}_{ab}^* and \bar{C}_{ab}^* , but when Alice moves a certain distance away from Willie, the OM transmission mode is better. On the one hand, the power received by Bob is smaller due to the rapid attenuation of mmWave; on the other hand, Willie is in the main lobe radiation range such that Willie has good detection performance. By comparing the two modes, we can derive the optimal transmission mode as Fig. 10 in the hybrid microwave/mmWave A2G Systems.

VIII. CONCLUSION

This paper investigated the covert communication in a hybrid Microwave/mmWave A2G wireless communication system. Based on our theoretical performance analysis and covert performance optimization under both OM and DM transmission modes, we proposed a new hybrid OM/DM transmission mode for covert performance enhancement. The results in this paper revealed that the hybrid transmission mode can lead to a significant improvement of overt performance than the pure OM or DM mode in the concerned A2G system. It is expected that this work can provide meaningful insights into the covert communication scheme design in more general and more complicated UAV networks, e.g., UAV with multiple band antennas, UAV swarm, etc.

APPENDIX A PROOF OF LEMMA 2

Here, we provide the calculation steps for (27) as follows

$$\int_0^a x f_{|h_{aw}^{o,\mathbb{B}}|^2}(x) dx = x F_{|h_{aw}^{o,\mathbb{B}}|^2}(x) \Big|_0^a - \int_0^a F_{|h_{aw}^{o,\mathbb{B}}|^2}(x) dx. \quad (65)$$

Similarly to (35), we can derive the first term on the right as

$$x F_{|h_{aw}^{o,\mathbb{B}}|^2}(x) \Big|_0^a = a \left(1 - \exp \left(- [2a(k_{\mathbb{B}} + 1)]^{\frac{\nu(\sqrt{2k_{\mathbb{B}}})}{2}} e^{\mu(\sqrt{2k_{\mathbb{B}}})} \right) \right). \quad (66)$$

Then, we derive the second term on the right as

$$\begin{aligned} \int_0^a F_{|h_{aw}^{o,\mathbb{B}}|^2}(x) dx &= \int_0^a 1 - \exp \left(- [2x(k_{\mathbb{B}} + 1)]^{\frac{\nu(\sqrt{2k_{\mathbb{B}}})}{2}} e^{\mu(\sqrt{2k_{\mathbb{B}}})} \right) dx \\ &= a - \int_0^a \exp \left(- [2x(k_{\mathbb{B}} + 1)]^{\frac{\nu(\sqrt{2k_{\mathbb{B}}})}{2}} e^{\mu(\sqrt{2k_{\mathbb{B}}})} \right) dx \\ &\stackrel{(a)}{=} a - \frac{\gamma \left(\frac{2}{\nu(\sqrt{2k_{\mathbb{B}}})}, [2a(k_{\mathbb{B}} + 1)]^{\frac{\nu(\sqrt{2k_{\mathbb{B}}})}{2}} e^{\mu(\sqrt{2k_{\mathbb{B}}})} \right)}{(k_{\mathbb{B}} + 1)\nu(\sqrt{2k_{\mathbb{B}}}) e^{\frac{2\mu(\sqrt{2k_{\mathbb{B}}})}{\nu(\sqrt{2k_{\mathbb{B}}})}}}, \end{aligned} \quad (67)$$

where step (a) is according to $\int_0^u x^m e^{-bx^n} dx = \frac{\gamma(v, bu^n)}{nb^n v}$, $v = \frac{m+1}{n}$ as in [52, Eq. (3.381.8)]. Substituting (66) and (67) into (65), we can obtain (27).

APPENDIX B PROOF OF LEMMA 4

Here, we provide the calculation steps for (47) as follows

$$\int_0^a x f_{|h_{aw}^{m,\mathbb{B}}|^2}(x) dx = x F_{|h_{aw}^{m,\mathbb{B}}|^2}(x) \Big|_0^a - \int_0^a F_{|h_{aw}^{m,\mathbb{B}}|^2}(x) dx. \quad (68)$$

According to (9), we can derive the first term on the right as

$$x F_{|h_{aw}^{m,\mathbb{B}}|^2}(x) \Big|_0^a = a \sum_{r=0}^{S_{\mathbb{B}}} \binom{S_{\mathbb{B}}}{r} (-1)^r e^{-r\xi_{\mathbb{B}} a}. \quad (69)$$

Similarly, the second term on the right can be derived as

$$\begin{aligned} \int_0^a F_{|h_{aw}^{m,\mathbb{B}}|^2}(x) dx &= \int_0^a \sum_{r=0}^{S_{\mathbb{B}}} \binom{S_{\mathbb{B}}}{r} (-1)^r e^{-r\xi_{\mathbb{B}} x} dx \\ &= \int_0^a \left[1 + \sum_{r=1}^{S_{\mathbb{B}}} \binom{S_{\mathbb{B}}}{r} (-1)^r e^{-r\xi_{\mathbb{B}} x} \right] dx \\ &= a + \sum_{r=1}^{S_{\mathbb{B}}} \binom{S_{\mathbb{B}}}{r} \frac{(-1)^r}{r\xi_{\mathbb{B}}} (1 - e^{-r\xi_{\mathbb{B}} a}). \end{aligned} \quad (70)$$

Then, substituting (69) and (70) into (68), we can obtain (47).

REFERENCES

- [1] L. Chen, L. Chen, S. Jordan, Y.-K. Liu, D. Moody, R. Peralta, R. Perlner, and D. Smith-Tone, *Report on post-quantum cryptography*. US Department of Commerce, National Institute of Standards and Technology, 2016, vol. 12.
- [2] X. Zhou, L. Song, and Y. Zhang, *Physical layer security in wireless communications*. CRC Press, 2013.
- [3] S. Yan, X. Zhou, J. Hu, and S. V. Hanly, "Low probability of detection communication: Opportunities and challenges," *IEEE Wireless Commun.*, vol. 26, no. 5, pp. 19–25, Oct. 2019.
- [4] B. A. Bash, D. Goeckel, and D. Towsley, "Limits of reliable communication with low probability of detection on AWGN channels," *IEEE J. Sel. Areas Commun.*, vol. 31, no. 9, pp. 1921–1930, Aug. 2013.
- [5] P. H. Che, M. Bakshi, and S. Jaggi, "Reliable deniable communication: Hiding messages in noise," in *Proc. IEEE Int. Symp. Info. Theory*, Oct. 2013, pp. 2945–2949.

- [6] L. Wang, G. W. Wornell, and L. Zheng, "Fundamental limits of communication with low probability of detection," *IEEE Trans. Inf. Theory*, vol. 62, no. 6, pp. 3493–3503, Jun. 2016.
- [7] A. Abdelaziz and C. E. Koksai, "Fundamental limits of covert communication over MIMO AWGN channel," in *Proc. IEEE Conf. Commun. Network Security*, Dec. 2017, pp. 1–9.
- [8] S. Lee, R. J. Baxley, M. A. Weitnauer, and B. Walkenhorst, "Achieving undetectable communication," *IEEE J. Sel. Top. Signal Process.*, vol. 9, no. 7, pp. 1195–1205, Apr. 2015.
- [9] K. Li, P. A. Kelly, and D. Goeckel, "Optimal power adaptation in covert wireless communication with an uninformed jammer," *IEEE Trans. Wireless Commun.*, vol. 19, no. 5, pp. 3463–3473, Feb. 2020.
- [10] K. Shahzad and X. Zhou, "Covert wireless communications under quasi-static fading with channel uncertainty," *IEEE Trans. Inf. Forensics Secur.*, vol. 16, pp. 1104–1116, Oct. 2020.
- [11] K. Shahzad, X. Zhou, and S. Yan, "Covert communication in fading channels under channel uncertainty," in *Proc. IEEE 85th Veh. Technol. Conf.*, Jun. 2017, pp. 1–5.
- [12] K. Shahzad, X. Zhou, S. Yan, J. Hu, F. Shu, and J. Li, "Achieving covert wireless communications using a full-duplex receiver," *IEEE Trans. Wireless Commun.*, vol. 17, no. 12, pp. 8517–8530, Nov. 2018.
- [13] R. Soltani, D. Goeckel, D. Towsley, B. A. Bash, and S. Guha, "Covert wireless communication with artificial noise generation," *IEEE Trans. Wireless Commun.*, vol. 17, no. 11, pp. 7252–7267, Nov. 2018.
- [14] T.-X. Zheng, H.-M. Wang, D. W. K. Ng, and J. Yuan, "Multi-antenna covert communications in random wireless networks," *IEEE Trans. Wireless Commun.*, vol. 18, no. 3, pp. 1974–1987, Feb. 2019.
- [15] J. Bai, J. He, Y. Chen, Y. Shen, and X. Jiang, "On covert communication performance with outdated CSI in wireless greedy relay systems," *IEEE Trans. Inf. Forensics Secur.*, vol. 17, pp. 2920–2935, Aug. 2022.
- [16] L. Lv, Q. Wu, Z. Li, Z. Ding, N. Al-Dhahir, and J. Chen, "Covert communication in intelligent reflecting surface-assisted NOMA systems: Design, analysis, and optimization," *IEEE Trans. Wireless Commun.*, vol. 21, no. 3, pp. 1735–1750, Aug. 2021.
- [17] M. T. Mamaghani and Y. Hong, "Aerial intelligent reflecting surface enabled terahertz covert communications in beyond-5G Internet of Things," *IEEE Internet Things J.*, vol. 9, no. 19, pp. 19012–19033, Mar. 2022.
- [18] M. V. Jamali and H. Mahdaviyar, "Covert millimeter-wave communication: Design strategies and performance analysis," *IEEE Trans. Wireless Commun.*, Nov. 2021.
- [19] J. Zhang, M. Li, S. Yan, C. Liu, X. Chen, M.-J. Zhao, and P. Whiting, "Joint beam training and data transmission design for covert millimeter-wave communication," *IEEE Trans. Inf. Forensics Secur.*, vol. 16, pp. 2232–2245, Jan. 2021.
- [20] J. Zhang, M. Li, M.-J. Zhao, X. Ji, and W. Xu, "Multi-user beam training and transmission design for covert millimeter-wave communication," *IEEE Trans. Inf. Forensics Secur.*, vol. 17, pp. 1528–1543, Mar. 2022.
- [21] C. Wang, Z. Li, and D. W. K. Ng, "Covert rate optimization of millimeter wave full-duplex communications," *IEEE Trans. Wireless Commun.*, vol. 21, no. 5, pp. 2844–2861, Oct. 2021.
- [22] H.-S. Im and S.-H. Lee, "Mobility-assisted covert communication over wireless ad hoc networks," *IEEE Trans. Inf. Forensics Secur.*, vol. 16, pp. 1768–1781, Dec. 2020.
- [23] B. Yang, T. Taleb, Y. Fan, and S. Shen, "Mode selection and cooperative jamming for covert communication in D2D underlaid UAV networks," *IEEE Network*, vol. 35, no. 2, pp. 104–111, Feb. 2021.
- [24] X. Zhou, S. Yan, J. Hu, J. Sun, J. Li, and F. Shu, "Joint optimization of a UAV's trajectory and transmit power for covert communications," *IEEE Trans. Signal Process.*, vol. 67, no. 16, pp. 4276–4290, Jul. 2019.
- [25] X. Zhou, S. Yan, D. W. K. Ng, and R. Schober, "Three-dimensional placement and transmit power design for UAV covert communications," *IEEE Trans. Veh. Technol.*, vol. 70, no. 12, pp. 13 424–13 429, Oct. 2021.
- [26] X. Chen, M. Sheng, N. Zhao, W. Xu, and D. Niyato, "UAV-relayed covert communication towards a flying warden," *IEEE Trans. Commun.*, vol. 69, no. 11, pp. 7659–7672, Aug. 2021.
- [27] X. Zhou, S. Yan, F. Shu, R. Chen, and J. Li, "UAV-enabled covert wireless data collection," *IEEE J. Sel. Areas Commun.*, vol. 39, no. 11, pp. 3348–3362, Jun. 2021.
- [28] Z. Li, X. Liao, J. Shi, L. Li, and P. Xiao, "MD-GAN based UAV trajectory and power optimization for cognitive covert communications," *IEEE Internet Things J.*, Oct. 2021.
- [29] H. Rao, S. Xiao, S. Yan, J. Wang, and W. Tang, "Optimal geometric solutions to UAV-enabled covert communications in line-of-sight scenarios," *IEEE Trans. Wireless Commun.*, June 2022.
- [30] J. Hu, Y. Wu, R. Chen, F. Shu, and J. Wang, "Optimal detection of UAV's transmission with beam sweeping in covert wireless networks," *IEEE Trans. Veh. Technol.*, vol. 69, no. 1, pp. 1080–1085, Oct. 2019.
- [31] H.-M. Wang, Y. Zhang, X. Zhang, and Z. Li, "Secrecy and covert communications against UAV surveillance via multi-hop networks," *IEEE Trans. Commun.*, vol. 68, no. 1, pp. 389–401, Nov. 2019.
- [32] J. Zhang, X. Chen, M. Li, and M. Zhao, "Optimized throughput in covert millimeter-wave UAV communications with beam sweeping," *IEEE Wireless Commun. Lett.*, vol. 10, no. 4, pp. 720–724, Dec. 2020.
- [33] M. T. Mamaghani and Y. Hong, "Aerial intelligent reflecting surface enabled terahertz covert communications in beyond-5G Internet of Things," *IEEE Internet Things J.*, vol. 9, no. 19, pp. 19012–19033, Mar. 2022.
- [34] B. J. Xiang, S. Y. Zheng, H. Wong, Y. M. Pan, K. X. Wang, and M. H. Xia, "A flexible dual-band antenna with large frequency ratio and different radiation properties over the two bands," *IEEE Trans. Antennas Propag.*, vol. 66, no. 2, pp. 657–667, 2017.
- [35] J. F. Zhang, Y. J. Cheng, Y. R. Ding, and C. X. Bai, "A dual-band shared-aperture antenna with large frequency ratio, high aperture reuse efficiency, and high channel isolation," *IEEE Trans. Antennas Propag.*, vol. 67, no. 2, pp. 853–860, 2018.
- [36] Y. Li and J. Wang, "Dual-band leaky-wave antenna based on dual-mode composite microstrip line for microwave and millimeter-wave applications," *IEEE Trans. Antennas Propag.*, vol. 66, no. 4, pp. 1660–1668, Feb. 2018.
- [37] S. Vuppala, S. Biswas, and T. Ratnarajah, "An analysis on secure communication in millimeter/micro-wave hybrid networks," *IEEE Trans. Commun.*, vol. 64, no. 8, pp. 3507–3519, 2016.
- [38] O. Semiari, W. Saad, and M. Bennis, "Joint millimeter wave and microwave resources allocation in cellular networks with dual-mode base stations," *IEEE Trans. Wireless Commun.*, vol. 16, no. 7, pp. 4802–4816, May 2017.
- [39] K. Venugopal, M. C. Valenti, and R. W. Heath, "Device-to-device millimeter wave communications: Interference, coverage, rate, and finite topologies," *IEEE Trans. Wireless Commun.*, vol. 15, no. 9, pp. 6175–6188, June 2016.
- [40] Y. Zhu, G. Zheng, and M. Fitch, "Secrecy rate analysis of UAV-enabled mmwave networks using Matérn hardcore point processes," *IEEE J. Sel. Areas Commun.*, vol. 36, no. 7, pp. 1397–1409, Apr. 2018.
- [41] J. G. Andrews, T. Bai, M. N. Kulkarni, A. Alkhateeb, A. K. Gupta, and R. W. Heath, "Modeling and analyzing millimeter wave cellular systems," *IEEE Trans. Commun.*, vol. 65, no. 1, pp. 403–430, Oct. 2016.
- [42] A. Al-Hourani, S. Kandeepan, and S. Lardner, "Optimal LAP altitude for maximum coverage," *IEEE Wireless Commun. Lett.*, vol. 3, no. 6, pp. 569–572, July 2014.
- [43] S. Shimamoto *et al.*, "Channel characterization and performance evaluation of mobile communication employing stratospheric platforms," *IEICE Trans. Commun.*, vol. 89, no. 3, pp. 937–944, Mar. 2006.
- [44] C. You and R. Zhang, "3D trajectory optimization in Rician fading for UAV-enabled data harvesting," *IEEE Trans. Wireless Commun.*, vol. 18, no. 6, pp. 3192–3207, Apr. 2019.
- [45] M. K. Simon and M.-S. Alouini, *Digital communication over fading channels*. John Wiley & Sons, 2005, vol. 95.
- [46] T. Bai and R. W. Heath, "Coverage and rate analysis for millimeter-wave cellular networks," *IEEE Trans. Wireless Commun.*, vol. 14, no. 2, pp. 1100–1114, Oct. 2014.
- [47] H. Alzer, "On some inequalities for the incomplete gamma function," *Math. Comp.*, vol. 66, no. 218, pp. 771–778, 1997.
- [48] S. Shellhammer, "Performance of the power detector with noise uncertainty," *Doc. IEEE 802.22-06/0134r0*, 2006.
- [49] A. Browder, *Mathematical analysis: an introduction*. Springer Science & Business Media, 2012.
- [50] D. Mishra and S. De, "i²RES: Integrated information relay and energy supply assisted RF harvesting communication," *IEEE Trans. Commun.*, vol. 65, no. 3, pp. 1274–1288, Dec. 2016.
- [51] M. Z. Bocus, C. P. Dettmann, and J. P. Coon, "An approximation of the first order Marcum Q-function with application to network connectivity analysis," *IEEE Commun. Lett.*, vol. 17, no. 3, pp. 499–502, Jan. 2013.
- [52] I. S. Gradshteyn and I. M. Ryzhik, *Table of integrals, series, and products*. Academic press, 2014.
- [53] M. R. Akdeniz, Y. Liu, M. K. Samimi, S. Sun, S. Rangan, T. S. Rappaport, and E. Erkip, "Millimeter wave channel modeling and cellular capacity evaluation," *IEEE J. Sel. Areas Commun.*, vol. 32, no. 6, pp. 1164–1179, Jun. 2014.
- [54] C. Liu, M. Li, S. V. Hanly, I. B. Collings, and P. Whiting, "Millimeter wave beam alignment: Large deviations analysis and design insights," *IEEE J. Sel. Areas Commun.*, vol. 35, no. 7, pp. 1619–1631, Apr. 2017.